2007

Nonlinear vibration of a cantilever beam

Iván Delgado-Velázquez

Nonlinear Vibration of a Cantilever Beam

by
Iván Delgado-Velázquez

A thesis submitted in partial fulfillment of the
requirements for the degree of

MASTER OF SCIENCE
IN
MECHANICAL ENGINEERING

Dr. Hany Ghoneim
Department of Mechanical Engineering _____ (Thesis Advisor)

Dr. Lawrence Agbezuge
Department of Mechanical Engineering _____

Dr. David Ross
School of Mathematical Sciences _____

Dr. Edward C. Hensel
Department of Mechanical Engineering _____

DEPARTMENT OF MECHANICAL ENGINEERING
ROCHESTER INSTITUTE OF TECHNOLOGY

2007

Nonlinear Vibration of a Cantilever Beam

I, _____, hereby **deny permission** to the RIT Library of the Rochester Institute of Technology to reproduce my print thesis or dissertation in whole or in part.

Signature of Author: _____ Date:_____

Nonlinear Vibration of a Cantilever Beam

By

Iván Delgado-Velázquez

Master of Science in Mechanical Engineering

Abstract

The vibration of a highly flexible cantilever beam is investigated. The order three equations of motion, developed by Crespo da Silva and Glyn (1978), for the nonlinear flexural-flexural-torsional vibration of inextensional beams, are used to investigate the time response of the beam subjected to harmonic excitation at the base. The equation for the planar flexural vibration of the beam is solved using the finite element method. The finite element model developed in this work employs Galerkin's weighted residuals method, combined with the Newmark technique, and an iterative process. This finite element model is implemented in the program *NLB*[1], which is used to calculate the steady state and transient responses of the beam. The steady state response obtained with *NLB* is compared to the experimental response obtained by Malatkar (2003). Some disagreement is observed between the numerical and experimental steady state responses, due to the presence of numerical error in the calculation of the nonlinear inertia term in the former. The transient response obtained with *NLB* reasonably agrees with the response calculated with ANSYS®.

Keywords: nonlinear vibration, cantilever beam

[1] Non Linear Beam

To Jesus Christ, my living Savior. Thanks to your power
in my life I am able to conquer anything. You are the music in my heart.

A Mamita Aida, Papito Rubén y Carly. Gracias por su amor y enseñanza.

A mi esposa Dara. Tu amor ha sido mi inspiración para llegar a la meta.

To Sylvia and Dana. Thank you for loving me as a son and a brother.

Acknowledgements

First I would like to thank my thesis advisor, Dr. Hany Ghoneim, for his guidance and support. I would also like to thank the members of my thesis committee: Dr. Lawrence Agbezuge , Dr. David Ross, and Dr. Edward C. Hensel for taking time to review my work. Finally, I would like to thank Xerox Corporation for providing me with the time and financial resources to complete this degree.

Table of Contents

List of Figures

List of Tables

List of Variables and Abbreviations

A- constant
a- total number of grid points
A- cross sectional area
$A1_{ij}$- linear Newmark matrix
$a1_{ij}$- nonlinear Newmark matrix
$A2_{ij}$- linear Newmark matrix
$a2_{ij}$- nonlinear Newmark matrix
$A3_{ij}$- linear Newmark matrix
$a3_{ij}$- nonlinear Newmark matrix
a_b- maximum amplitude of acceleration applied to the base of the beam
A_r- constant in normalized mode shapes
a_r- constant in the response of the beam to base excitation
A_α ($\alpha = \psi, \theta, \phi$)- group of terms in the equations of motion
B- constant
b- width of beam
BC- boundary conditions
b_i^e - element boundary vector
b_i- global boundary vector
b_r- constant in the response of the beam to base excitation
C- arbitrary point along the neutral axis in the undeformed configuration
C- constant
c_{ij}^e - nonlinear element damping matrix
c_{ij}^r - reduced global nonlinear damping matrix
$\overrightarrow{CP}$ - vector through points C and P
$\overrightarrow{C^*P^*}$ - vector through points C^* and P^*
C^*- arbitrary point along neutral axis in the deformed configuration
C^*D^*- deformed segment of neutral axis
CD- undeformed segment of neutral axis
C_{ij}- global linear damping matrix
c_{ij}- global nonlinear damping matrix
c_α ($\alpha = u, v, w$)- damping coefficient
D- constant
$d\vec{r}_P$ - distance differential of vector $\vec{r}_P$
$d\vec{r}_{P^*}$ - distance differential of vector $\vec{r}_{P^*}$
ds- length of undeformed segment of neutral axis
ds^*- length of deformed segment of neutral axis
D_α ($\alpha = \xi, \eta, \zeta$)- flexural rigidity about α axis
e- strain at a point
E- Young's modulus
$\boldsymbol{e}_{\boldsymbol{\alpha}}$ ($\alpha = x, y, y', z, \xi, \eta, \zeta$)- unit vector along α axis
F_1^r - constant in the response of the beam to base excitation

F_i^d - dth linear force vector

F_i^e - element force vector

F- forcing function in equation of motion

f_i^r - reduced global nonlinear force vector

F_2^r - time dependent function in the response of the beam to base excitation

$f(x,t)$- forcing function in equation of motion

$\mathcal{F}_e$- elastic force

f_1- function accounting for the curvature nonlinear effect

f_2- function accounting for the inertial nonlinear effect

f_3- function accounting for the gravitational nonlinear effect

$\mathcal{F}_a$- inertial force

$\boldsymbol{f}_i$- nonlinear force vector discretized in the time domain

$\mathcal{F}_i$- linear force vector discretized in the time domain

F_i- global linear force vector

f_i- global nonlinear force vector

f_i^e - reduced nonlinear force vector

f_n- natural frequency in Hz

g- acceleration due to gravity

g_i- global gravitational effect vector

g_i^e - element gravitational effect vector

G- shear modulus

G_α (α= u, v, w)- group of terms in equations of motion

h- length of element

h- thickness of beam

$h(t)$- unit impulse response

$H.O.T.$- higher order terms

H_α (α= u, v, w)- group of terms in equation of motion

I- action integral

I- area moment of inertia

$I_1(s_k)$- first integral in f_2 evaluated at kth grid point

I_r- integral in A_r calculation

j- time node index

$J_j(s)$- second time derivative of v'^2 evaluated at jth time node

[J]- distributed inertia matrix

J_α (α=ξ, η, ζ)- moment of inertia about α axis

kc_{ij}^e - element nonlinear stiffness matrix for curvature effect

kc_{ij}- global nonlinear stiffness matrix for curvature effect

ki_{ij}^e - element nonlinear stiffness matrix for inertial effect

ki_{ij}- global nonlinear stiffness matrix for inertial effect

K_{ij}- global linear stiffness matrix

K_{ij}^e - linear element stiffness matrix

k_{ij}^r - reduced global nonlinear stiffness matrix

k_{ij}- global nonlinear stiffness matrix
$\boldsymbol{\ell}$- Lagrangian density
$\boldsymbol{\mathcal{L}}$- Lagrangian of motion
l- length of beam
$\boldsymbol{\mathcal{M}}$- bending moment
M_{ij}- global linear mass matrix
M_{ij}^{e} - linear element mass matrix
m- mass per unit length of beam
M_{ij}^{r} - reduced global linear mass matrix
N- number of elements
NLB- Non Linear Beam Matlab® program
$\overrightarrow{OC}$ - vector through points O and C
$\overrightarrow{OC^{*}}$ - vector through points O and C^{*}
P- point in the cross section of the undeformed beam
P^{*}- point in the cross section of the deformed beam
Q_{α}^{*} $(\alpha= u, v, w)$- generalized non conservative force
Q_{j}^{d} - dth linear displacement vector
q_{j}^{d} - dth nonlinear displacement vector
Q_{j}^{e} - element linear nodal displacement vector
q_{j}^{e} - element nonlinear nodal displacement vector
q'_{j}- nodal degree of freedom
q_{j}- global displacement vector
Q_{j}- nodal degree of freedom
Q_{j}- linear global displacement vector
q_{j}- nodal degree of freedom
$Q_{r}(t)$- forcing term
$q_{r}(t)$- time dependent component of forced linear response
Q_{α} $(\alpha= u, v, w, \phi)$- generalized force
$\overrightarrow{r_{P}}$ - position vector of point P
$\overrightarrow{r_{P^{*}}}$ - position vector of point P^{*}
R_{t}- residual for discretization in time domain
R_{x}- residual for discretization in spatial coordinate
s- coordinate along neutral axis
s- local s coordinate
S- global s coordinate
s_{k}- s coordinate of kth grid point along the beam
T- kinetic energy
t- time coordinate
[T]- transformation matrix
$[T_{\alpha}]$ $(\alpha= \psi, \theta, \phi)$ - transformation matrix for rotation by angle α
TF- final time in [0,TF]
TN- total number of time nodes

TOL- maximum allowable error for iterative procedure in *NLB*
T_{rot}- kinetic energy due to rotation
T_{tr}- kinetic energy due to translation
U- strain energy
u(s,t)- axial displacement
$\widetilde{V}^{e}(s,t)$ - displacement inside the elements
${}^{*}V_{r}(x)$ - normalized linear mode shapes
V- potential energy
$\mathcal{V}$- shear force
v(s,t)- transverse displacement in the *y* direction
V(t)- excitation at base of beam
V(x)- transverse displacement of beam
v_0- maximum amplitude of displacement applied to the base of the beam
v_b- transverse displacement relative to the base of the beam
${}^{j}v'$- spatial derivative of *v* evaluated at j^{th} time node
w(s,t)- transverse displacement in the *z* direction
$\mathcal{W}_s$ - weight of the beam above point *s* along neutral axis
W_{NC}- work done by non conservative forces
WR- weighted residual
x- coordinate in the inertial system
x'- new position of *x* axis
xyz- inertial coordinate system
y- coordinate in the inertial system
Y- global *y* coordinate
y'- new position of *y* axis
z- coordinate in the inertial system
z''- new position of *z* axis
Δt- time step
Δx- length of subdivision of the element
Φ_d- d^{th} shape function for discretization in time domain
Ω- excitation frequency
$\alpha(0,t)$- boundary conditions for fixed end of beam *(α= u, v, w, γ, v', w')*
$\alpha(l,t)$- boundary conditions for free end of beam *(α= u, v, w, γ, v', w')*
α_1- coefficient for proportional damping
α_2- coefficient for proportional damping
β- constant for Newmark technique
β- parameter in analytical solution of linear problem
δ_{rs}- Kronecker delta
$[\varepsilon_{ij}]$- Green's strain tensor
ε_{ij}- normal strain component in Green's strain tensor
ε_r- constant in analytical linear response
ϕ- Euler angle
$\phi(s,t)$- torsional angle
γ- angle of twist
γ- constant for Newmark technique

γ_{ij}- shear strain component in Green's strain tensor
η- coordinate in non inertial system
$\lambda(s,t)$- Lagrange multiplier
ν- non dimensional time coordinate
θ- error in the displacement
θ- Euler angle
θ- the product βl
θ_r- r^{th} value of θ
ρ- density
$\rho(s,t)$- curvature vector
ρ_α ($\alpha = \xi, \eta, \zeta$)- component of the curvature vector
σ_{ij}- component of stress tensor
τ- integration variable in convolution integral
ω- frequency of vibration
$\omega(s,t)$- angular velocity vector
$\omega(t)$- weighting function
ω_r- r^{th} natural frequency
ω_α ($\alpha = \xi, \eta, \zeta$)- component of angular velocity vector
ξ- coordinate in non inertial system
ξ_r- r^{th} modal damping ratio
$\xi\eta\zeta$- non inertial coordinate system
ψ- Euler angle
ψ_α ($\alpha = 1,2,3,4$)- shape functions for discretization in the spatial coordinate
ζ- coordinate in non inertial system

Chapter 1: Introduction

1.1 Introduction

A beam is an elongated member, usually slender, intended to resist lateral loads by bending (Cook, 1999). Structures such as antennas, helicopter rotor blades, aircraft wings, towers and high rise buildings are examples of beams. These beam-like structures are typically subjected to dynamic loads. Therefore, the vibration of beams is of particular interest to the engineer.

For beams undergoing small displacements, linear beam theory can be used to calculate the natural frequencies, mode shapes, and the response for a given excitation. However, when the displacements are large, linear beam theory fails to accurately describe the dynamic characteristics of the system.

Highly flexible beams, typically found in aerospace applications, may experience large displacements. These large displacements cause geometric and other nonlinearities to be significant. The nonlinearities couple the (linearly uncoupled) modes of vibration and can lead to modal interactions where energy is transferred between modes (Nayfeh, 1993).

This investigation focuses in the study of the time response of a highly flexible cantilever beam, subjected to harmonic excitation at the base. The equation for the planar flexural vibration of beams, derived by Crespo da Silva and Glyn (1978), is solved using the finite element method. The finite element model developed in this work employs Galerkin's weighted residuals method, combined with the Newmark technique, and an iterative process.

The vibration of highly flexible beams is well documented in the literature. A summary of relevant research is presented next.

1.2 Literature Review

Crespo da Silva and Glyn (1978) derived a set of integro-differential equations describing the nonlinear flexural-flexural-torsional vibration of inextensional beams. Their mathematical model includes nonlinear effects up to order three, such as the curvature and inertia effects. Crespo da Silva and Glyn used their model to investigate the non-planar oscillations of a cantilever beam (1979), and the out of plane vibration of a clamped-clamped/sliding beam subjected to planar excitation with support asymmetry (1979).

Anderson, et al. (1992) conducted experiments on a flexible cantilever beam subjected to harmonic excitation along the axis of the beam. Their investigation demonstrated that energy from a high-frequency excitation can be transferred to a low-frequency mode of a structure through two mechanisms: a combination resonance and a resonance due to modulations of the amplitudes and phases of the high-frequency modes. Anderson, et al. (1992) also investigated the response of a flexible cantilever beam subjected to random base excitation. Their results demonstrate that energy from a high frequency excitation can be transferred to a low-frequency mode of the beam.

Nayfeh and Nayfeh (1993) investigated the interaction between high and low frequency modes in a two degree of freedom nonlinear system. Nayfeh and Arafat (1998) studied the nonlinear flexural responses of cantilever beams to combination parametric and subcombination resonances.

Malatkar and Nayfeh (2003) performed an experimental and theoretical study of the response of a flexible cantilever beam to an external harmonic excitation near the third natural frequency of the beam. Their investigation reveals the response of the beam consists of an amplitude and phase modulated high frequency component, and a low frequency component. Moreover, the modulation frequency of the high frequency component is equal to the low frequency component (Malatkar, 2003).

Kim, et al. (2006) investigated the non-planar response of a circular cantilever beam subjected to base harmonic excitation. Their results show that the inertia nonlinear effect dominates the response of high frequency modes.

1.3 Overview

An overview of the remaining chapters is presented next. Chapter 2 covers the derivation by Crespo da Silva and Glyn (1978) for the nonlinear flexural-flexural-torsional vibration of a cantilever beam. Chapter 3 presents the numerical algorithm used to solve the equation of motion for the planar vibration of the beam subjected to harmonic excitation at the base. The numerical algorithm in Chapter 3 is implemented in the program *NLB*[2] (Appendix A). Chapter 4 compares the steady state response calculated with *NLB* to experimental results obtained by Malatkar (2003). Chapter 4 also compares the transient response from *NLB* to the response obtained with ANSYS®. Chapter 5 presents the conclusion and suggestions for future work.

[2] Non Linear Beam

Chapter 2: Equations of Motion

The approach employed by Crespo da Silva and Glynn (1978) is used to derive the equations of motion for the flexural-flexural-torsional vibrations of a cantilever beam. The equations of motion are derived using the extended Hamilton's principle. These equations are then simplified to include nonlinear terms up to order three. The chapter concludes with the derivation of the order three equation for the forced planar flexural vibration of the beam. This equation will be used in subsequent chapters.

2.1 Dynamic System and Assumptions

The dynamic system (Figure 2.1) consists of a vertically mounted cantilever beam of length *l*, mass per unit length *m*, made of isotropic material. The beam is assumed to be a nonlinear elastic structure. A nonlinear elastic structure undergoes large deformations, but small strains (Malatkar, 2003). The beam is also assumed to be an Euler-Bernoulli beam. Hence the effects of rotary inertia, shear deformation and warping are neglected.

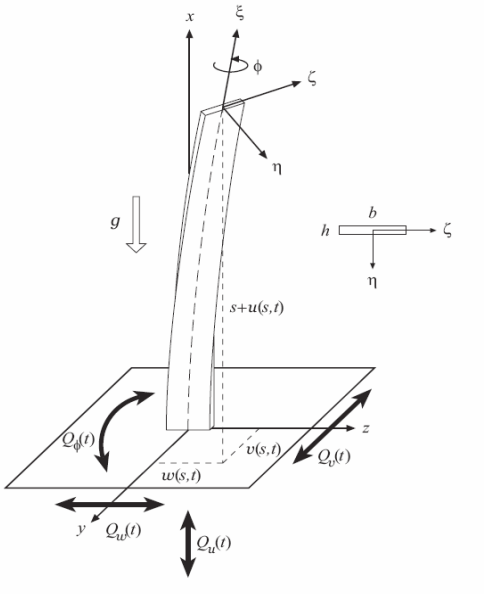

Figure 2. 1: Vertically mounted cantilever beam[3]

[3] Malatkar, 2003

Furthermore, the beam is idealized as an inextensional beam, i.e., there is no stretching of the neutral axis. Beams with one end fixed and the other end free can be assumed to be inextensional (Nayfeh and Pai, 2003).

Two coordinate systems are used to derive the equations of motion. The *x,y,* and *z* axes define the inertial coordinate system with orthogonal unit vectors $\boldsymbol{e}_x$, $\boldsymbol{e}_y$, and $\boldsymbol{e}_z$. The ξ, η and ζ axes define the local coordinate system with orthogonal unit vectors $\boldsymbol{e}_\xi$, $\boldsymbol{e}_\eta$ and $\boldsymbol{e}_\zeta$. The origin of this system is the centroid of the cross section at arc length *s*. The ζ and η axes are aligned with the principal axes of the cross section, while the ξ axis is aligned to the neutral axis of the beam. When the *x* and ξ axes are aligned with each other, the beam is in the undeformed position.

The beam is subjected to generalized forces Q_u, Q_v, Q_w, and Q_ϕ, which cause it to deform as shown in Figure 2.1. Since there is no warping of the cross section, any change of shape of the beam is due to rigid body motion. At any time, the deformed position of the beam consists of translation and rotation, which can be described in terms of the axial displacement *u(s,t)*; the flexural displacements *v(s,t)* and *w(s,t)*; and the torsional angle $\phi(s,t)$.

2.2 Euler Angles

In the undeformed configuration, the inertial coordinate system *xyz* is aligned with the $\xi\eta\zeta$ system. When the two coordinate systems are no longer aligned with each other, some deformation has taken place.

The transformation that the beam undergoes to get to the deformed state can be described in terms of three counterclockwise rigid body rotations. The Euler angles ψ, θ, and ϕ are used to describe these rotations.

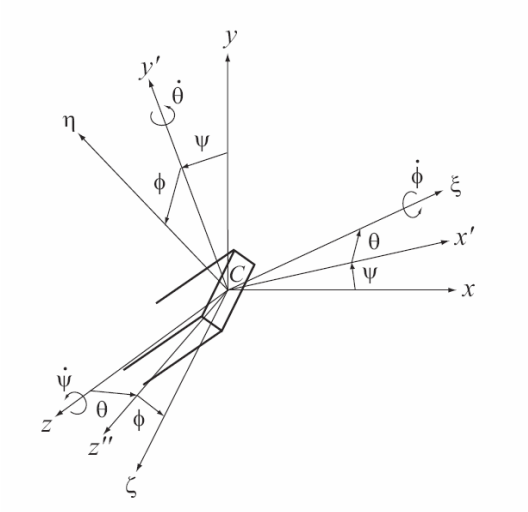

Figure 2. 2: Rigid body rotations of beam cross section[4]

Figure 2.2 shows the order in which the rotations are performed. First the *xyz* system is rotated about the *z* axis, then about *y′*, the new position of the *y* axis, and finally about the ξ axis. This order of rotation yields a set of equations of motion amenable to a study of moderately large amplitude flexural-torsional oscillations by perturbation techniques (Crespo da Silva, 1978).

The unit vectors of the $\xi\eta\zeta$ coordinate system are related to unit vectors of the *xyz* coordinate system through a transformation matrix [T]. The transformation matrix [T] is the product of three transformation matrices, one for each rigid body rotation.

$$\begin{bmatrix} \boldsymbol{e}_\xi \\ \boldsymbol{e}_\eta \\ \boldsymbol{e}_\zeta \end{bmatrix} = [T] \begin{bmatrix} \boldsymbol{e}_x \\ \boldsymbol{e}_y \\ \boldsymbol{e}_z \end{bmatrix} = [T_\phi][T_\theta][T_\psi] \begin{bmatrix} \boldsymbol{e}_x \\ \boldsymbol{e}_y \\ \boldsymbol{e}_z \end{bmatrix} \tag{2.1}$$

The three individual transformation matrices and the transformation matrix [T] are then

$$[T_\psi] = \begin{bmatrix} \cos\psi & \sin\psi & 0 \\ -\sin\psi & \cos\psi & 0 \\ 0 & 0 & 1 \end{bmatrix}, [T_\theta] = \begin{bmatrix} \cos\theta & 0 & -\sin\theta \\ 0 & 1 & 0 \\ \sin\theta & 0 & \cos\theta \end{bmatrix}, [T_\phi] = \begin{bmatrix} 1 & 0 & 0 \\ 0 & \cos\phi & \sin\phi \\ 0 & -\sin\phi & \cos\phi \end{bmatrix} \tag{2.2}$$

[4] Malatkar, 2003

$$[T]=\begin{bmatrix} \cos\theta\cos\psi & \cos\theta\sin\psi & -\sin\theta \\ -\sin\psi\cos\phi+\sin\phi\sin\theta\cos\psi & \cos\phi\cos\psi+\sin\phi\sin\theta\sin\psi & \sin\phi\cos\theta \\ \sin\phi\sin\psi+\cos\phi\sin\theta\cos\psi & -\sin\phi\cos\psi+\cos\phi\sin\theta\sin\psi & \cos\phi\cos\theta \end{bmatrix} \quad (2.3)$$

The absolute angular velocity of the local coordinate system $\xi\eta\zeta$ is obtained from Figure 2.2 . The overdot indicates differentiation with respect to time.

$$\omega(s,t)=\dot{\psi}\boldsymbol{e}_z+\dot{\theta}\boldsymbol{e}_{y'}+\dot{\phi}\boldsymbol{e}_\xi \quad (2.4)$$

The expressions for $\boldsymbol{e}_z$, and $\boldsymbol{e}_{y'}$ are easily obtained from the transformation matrices in (2.2) and (2.3).

$$\boldsymbol{e}_z=-\sin\theta\boldsymbol{e}_\xi+\sin\phi\cos\theta\boldsymbol{e}_\eta+\cos\phi\cos\theta\boldsymbol{e}_\zeta \quad (2.5)$$

$$\boldsymbol{e}_{y'}=\cos\phi\boldsymbol{e}_\eta-\sin\phi\boldsymbol{e}_\zeta \quad (2.6)$$

Substituting (2.5) and (2.6) into (2.4) yields

$$\omega(s,t)=(\dot{\phi}-\dot{\psi}\sin\theta)\boldsymbol{e}_\xi+(\dot{\psi}\sin\phi\cos\theta+\dot{\theta}\cos\phi)\boldsymbol{e}_\eta+(\dot{\psi}\cos\phi\cos\theta-\dot{\theta}\sin\phi)\boldsymbol{e}_\zeta \quad (2.7)$$

According to Kirchhoff's kinetic analogue (Love,1944), the curvature components can be obtained from the angular velocity components by replacing the time derivatives in (2.7) with spatial derivatives. Hence the curvature vector is given by

$$\rho(s,t)=(\phi'-\psi'\sin\theta)\boldsymbol{e}_\xi+(\psi'\sin\phi\cos\theta+\theta'\cos\phi)\boldsymbol{e}_\eta+(\psi'\cos\phi\cos\theta-\theta'\sin\phi)\boldsymbol{e}_\zeta \quad (2.8)$$

2.3 Inextensional Beam

Figure 2.3 shows a segment of the neutral axis of the cantilever beam. Segment *CD* is in the undeformed configuration while C^*D^* is in the deformed configuration. The strain at point *C* is given by

$$e = \frac{ds^* - ds}{ds} = \sqrt{(1+u')^2 + (v')^2 + (w')^2} - 1 \tag{2.9}$$

Since the beam is assumed to be inextensional, the strain along the neutral axis is zero. Therefore (2.9) becomes.

$$1 = (1+u')^2 + (v')^2 + (w')^2 \tag{2.10}$$

Equation (2.10) is reffered to as the *inextensionality constraint*.

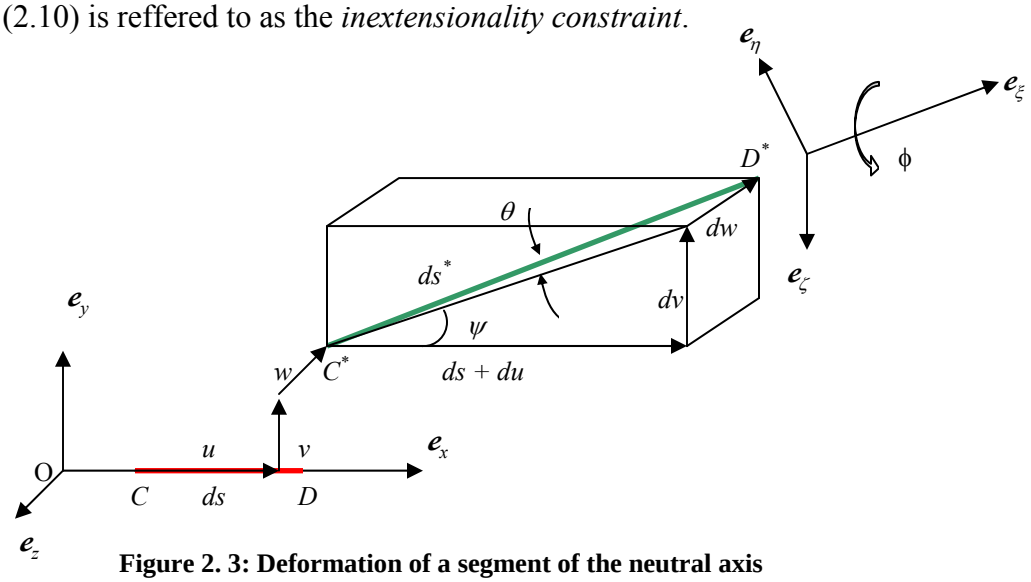

Figure 2. 3: Deformation of a segment of the neutral axis

Figure 2.3 can be used to determine the expressions for the angles ψ and θ in terms of the spatial derivatives of the transverse displacements. These expressions will be helpful in the simplification of the equations of motion later on. The relationships for ψ and θ are then

$$\tan\psi = \frac{v'}{1+u'}, \quad \tan\theta = \frac{-w'}{\sqrt{(1+u')^2 + (v')^2}} \tag{2.11}$$

Equation (2.11) indicates ψ and θ are dependent on the spatial derivatives of the displacement components *u, v,* and *w*. Therefore there are only four independent variables for this problem, namely *u, v, w,* and ϕ.

2.4 Strain-Curvature Relations

This section presents the derivation of the strain tensor components in terms of the curvature components. Figure 2.4 shows the beam cross section at arclength *s* for both the deformed and undeformed configurations.

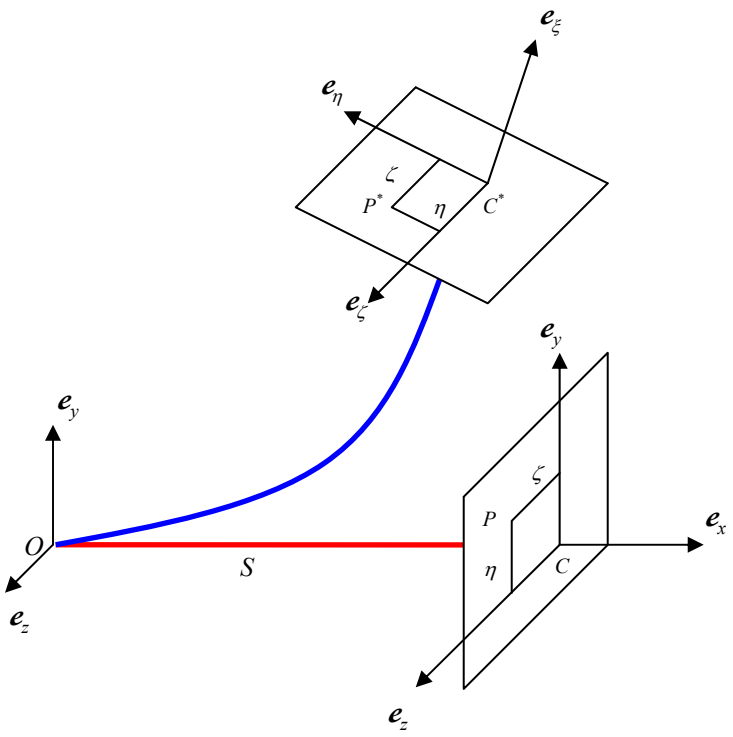

Figure 2. 4: Initial and deformed positions of an arbitrary point P

An arbitrary point P in the undeformed beam cross section moves to point P^* in the deformed cross section. The position vectors for points P and P^* are defined from Figure 2.4 as

$$\vec{r}_P = \overrightarrow{OC} + \overrightarrow{CP} = s\boldsymbol{e}_x + \eta\boldsymbol{e}_y + \zeta\boldsymbol{e}_z \tag{2.12}$$

$$\vec{r}_{P^*} = \overrightarrow{OC^*} + \overrightarrow{C^*P^*} = (s+u)\boldsymbol{e}_x + v\boldsymbol{e}_y + w\boldsymbol{e}_z + \eta\boldsymbol{e}_\eta + \zeta\boldsymbol{e}_\zeta \tag{2.13}$$

The distance differentials for points P and P^* are given by

$$d\vec{r}_P = ds\boldsymbol{e}_x + d\eta\boldsymbol{e}_y + d\zeta\boldsymbol{e}_z \tag{2.14}$$

$$d\vec{r}_{P^*} = ds\boldsymbol{e}_\xi + \eta d\boldsymbol{e}_\eta + d\eta\boldsymbol{e}_\eta + \varsigma d\boldsymbol{e}_\zeta + d\zeta\boldsymbol{e}_\zeta \tag{2.15}$$

with the first term in (2.15) given by

$$ds\boldsymbol{e}_\xi = (1+u')ds\boldsymbol{e}_x + v'ds\boldsymbol{e}_y + w'ds\boldsymbol{e}_z = C^*D^* \tag{2.16}$$

which is obtained directly from Figure 2.3. Equations (2.14) and (2.15) are used to obtain

$$d\vec{r}_{P*}\cdot d\vec{r}_{P*} - d\vec{r}_P\cdot d\vec{r}_P = 2(\zeta\rho_\eta - \eta\rho_\zeta)ds^2 - 2\zeta\rho_\xi ds d\eta + 2\eta\rho_\xi ds d\zeta + H.O.T. \tag{2.17}$$

where *H.O.T.* stands for higher order terms.

The difference of the squared distance differentials is related to the Green's strain tensor by (Mase, 1970)

$$d\vec{r}_{P*}\cdot d\vec{r}_{P*} - d\vec{r}_P\cdot d\vec{r}_P = 2\begin{bmatrix} ds & d\eta & d\zeta \end{bmatrix}\cdot\begin{bmatrix}\varepsilon_{ij}\end{bmatrix}\cdot\begin{bmatrix} ds & d\eta & d\zeta \end{bmatrix}^T \tag{2.18}$$

The components of the strain tensor in terms of the curvature are found by expanding the right hand side of (2.18) and comparing it to the right hand side of (2.17).

$$\varepsilon_{11} = \zeta\rho_{\eta} - \eta\rho_{\zeta}\,,\ \ \gamma_{12} = 2\varepsilon_{12} = -\zeta\rho_{\xi}\,,\ \ \gamma_{13} = 2\varepsilon_{13} = \eta\rho_{\xi}\,,\ \varepsilon_{22} = \varepsilon_{23} = \varepsilon_{33} = 0 \qquad (2.19)$$

2.5 Lagrangian of Motion

The Lagrangian of motion is defined as

$$\mathcal{L} = T - V = \int_0^l \ell \, ds \qquad (2.20)$$

where T is the kinetic energy, V the potential energy, l the length of the beam and ℓ the Lagrangian density.

The kinetic energy has two components, one due to translation and one due to rotation. The kinetic energy due to translation is given by

$$T_{tr} = \frac{1}{2} m \int_0^l (\dot{u}^2 + \dot{v}^2 + \dot{w}^2) ds \qquad (2.21)$$

The kinetic energy due to rotation is given by

$$T_{rot} = \frac{1}{2} \int_0^l [\omega_{\xi} \quad \omega_{\eta} \quad \omega_{\zeta}][J][\omega_{\xi} \quad \omega_{\eta} \quad \omega_{\zeta}]^T ds \qquad (2.22)$$

where [J] is the distributed inertia matrix. Because the local coordinate system coincides with the principal axes of the beam, the product moments of inertia are zero (Budynas, 1999). Therefore, the inertia matrix [J] is given by

$$[J]=\begin{bmatrix} J_\xi & 0 & 0 \\ 0 & J_\eta & 0 \\ 0 & 0 & J_\varsigma \end{bmatrix} \tag{2.23}$$

with the elements along the diagonal defined by

$$J_\xi = \iint_A \rho(\eta^2+\zeta^2)d\eta d\zeta\,,\;\; J_\eta = \iint_A \rho\zeta^2 d\eta d\zeta\,,\;\; J_\varsigma = \iint_A \rho\eta^2 d\eta d\zeta \tag{2.24}$$

Substituting (2.24) into (2.22), and adding (2.21) to the resulting expression yields the expression for the total kinetic energy of the system.

$$T = \frac{1}{2}\int_0^l [m(\dot{u}^2+\dot{v}^2+\dot{w}^2)+J_\xi\omega_\xi{}^2+J_\eta\omega_\eta{}^2+J_\varsigma\omega_\varsigma{}^2]\quad ds \tag{2.25}$$

The potential energy is equal to the strain energy of the beam, which is calculated using the strain tensor components in (2.19). Therefore, the total strain energy is given by

$$U = \frac{1}{2}\int_0^l \{\iint_A (\sigma_{11}\varepsilon_{11}+\sigma_{12}\gamma_{12}+\sigma_{13}\gamma_{13})d\eta d\zeta\} ds \tag{2.26}$$

For this derivation, a linear relationship between the stress and the strain is assumed. Therefore, Hooke's law can be used to relate the stress to the strain.

$$\sigma_{11} \approx E\varepsilon_{11}\,,\;\; \sigma_{12} \approx G\gamma_{12}\,,\;\; \sigma_{13} \approx G\gamma_{13} \tag{2.27}$$

Substituting the strain tensor components from the previous section into (2.26) and (2.27), and noting that the cross section is symmetric about the η and ζ axes, the strain energy is written as

$$U = \frac{1}{2}\int_0^l (D_\xi \rho_\xi^{\,2} + D_\eta \rho_\eta^{\,2} + D_\zeta \rho_\zeta^{\,2}) \quad ds \tag{2.28}$$

where D_ξ, D_η, and D_ζ are the torsional and flexural rigidities, respectively. The potential energy is then

$$V = \frac{1}{2}\int_0^l (D_\xi \rho_\xi^{\,2} + D_\eta \rho_\eta^{\,2} + D_\zeta \rho_\zeta^{\,2}) \quad ds \tag{2.29}$$

Equations (2.25) and (2.29) are substituted into (2.20) to obtain the final expression for the Lagrangian. The inextensionality constraint in (2.10) must be maintained during the variational process. To enforce this constraint, equation (2.10) is attached to the Lagrangian density by using a Lagrange multiplier $\lambda(s,t)$. The Lagrangian density is then

$$\begin{aligned} \ell = {} & \frac{1}{2} m(\dot{u}^2 + \dot{v}^2 + \dot{w}^2) + \frac{1}{2}(J_\xi \omega_\xi^{\,2} + J_\eta \omega_\eta^{\,2} + J_\zeta \omega_\zeta^{\,2}) \\ & - \frac{1}{2}(D_\xi \rho_\xi^{\,2} + D_\eta \rho_\eta^{\,2} + D_\zeta \rho_\zeta^{\,2}) + \frac{1}{2}\lambda[1 - (1+u')^2 - (v')^2 - (w')^2] \end{aligned} \tag{2.30}$$

The Lagragian resulting from substituting (2.30) into (2.20) is an example of an augmented functional. Variational problems dealing with finding the extremal of an augmented functional are known as *isoperimetric problems* (Török, 2000).

2.6 Extended Hamilton's Principle

The cantilever beam is subjected to non conservative forces such as viscous damping and the generalized forces Q_α (α=. *u, v, w,* and ϕ). Therefore, the extended

Hamilton's principle (Meirovitch, 2001) is used to derive the equations of motion. The extended Hamilton's principle can be stated as follows

$$\delta I = \int_{t_1}^{t_2} (\delta \mathcal{L} + \delta W_{NC}) = 0 \tag{2.31}$$

where $\delta \mathcal{L}$ is the virtual change in mechanical energy, and δW_{NC} the virtual work due to non conservative forces. The virtual work due to non conservative forces is given by

$$\delta W_{NC} = \int_0^l (Q^*_u \delta u + Q^*_v \delta v + Q^*_w \delta w + Q^*_\phi \delta \phi) ds \tag{2.32}$$

where Q^*_α ($\alpha = u, v, w,$ and ϕ) stands for the generalized non conservative forces defined as

$$Q^*_\alpha = Q_\alpha - c_\alpha \dot{\alpha} \tag{2.33}$$

The variation of the Lagrangian is given by

$$\delta \mathcal{L} = \int_0^l \delta \ell ds \tag{2.34}$$

The Lagrangian density is a functional of *13* variables, namely $u,v,w,\phi,$ their time and space derivatives, and the Lagrange multiplier λ. Therefore, the variation of the Lagrangian density is given by

$$\delta \ell = \sum_{i=1}^{13} \frac{\partial \ell}{\partial x_i} \delta x_i \tag{2.35}$$

Equation (2.11) in section 2.3 is used to obtain the variations of ψ and θ.

$$\delta\psi = \frac{\partial\psi}{\partial u'}\delta u' + \frac{\partial\psi}{\partial v'}\delta v' = \frac{-v'\delta u' + (1+u')\delta v'}{(1+u')^2 + (v')^2} \tag{2.36}$$

$$\delta\theta = \frac{\partial\theta}{\partial u'}\delta u' + \frac{\partial\theta}{\partial v'}\delta v' + \frac{\partial\theta}{\partial w'}\delta w' = \frac{w'[(1+u')\delta u' + v'\delta v']}{\sqrt{(1+u')^2 + (v')^2}} - \sqrt{(1+u')^2 + (v')^2}\,\delta w' \tag{2.37}$$

The preceding two equations are used to compute the variation of the Lagrangian density given by (2.35). Taking the variation of the Lagrangian density and integrating by parts several times results in

$$\begin{aligned}
&\int_{t_1}^{t_2}\{\int_0^l (-m\ddot{u} + Q^*{}_u + G'_u)\delta u\,ds + \int_0^l (-m\ddot{v} + Q^*{}_v + G'_v)\delta v\,ds + \\
&\quad \int_0^l (-m\ddot{w} + Q^*{}_w + G'_w)\delta w\,ds + \int_0^l (Q^*{}_\phi - A_\phi)\delta\phi\,ds + \\
&\quad \left[-G_u\delta u - G_v\delta v - G_w\delta w + H_u\delta u' + H_v\delta v' + H_w\delta w' + \frac{\partial \boldsymbol{\ell}}{\partial \phi'}\delta\phi\right]_{s=0}^{l}\}dt = 0
\end{aligned} \tag{2.38}$$

with G_u, G_v, and G_w given by

$$G_u = A_\psi\frac{\partial\psi}{\partial u'} + A_\theta\frac{\partial\theta}{\partial u'} + \lambda(1+u'),\quad G_v = A_\psi\frac{\partial\psi}{\partial v'} + A_\theta\frac{\partial\theta}{\partial v'} + \lambda v',\quad G_w = A_\theta\frac{\partial\theta}{\partial w'} + \lambda w' \tag{2.39}$$

and A_ψ, A_θ, A_ϕ, H_u, H_v, and H_w given by

$$\begin{aligned}
A_\alpha &= \frac{\partial^2 \boldsymbol{\ell}}{\partial t\partial\dot{\alpha}} + \frac{\partial^2 \boldsymbol{\ell}}{\partial s\partial\alpha'} - \frac{\partial \boldsymbol{\ell}}{\partial\alpha} \qquad (\alpha = \psi,\theta,\phi) \\
H_\alpha &= \frac{\partial \boldsymbol{\ell}}{\partial\psi'}\frac{\partial\psi}{\partial\alpha'} + \frac{\partial \boldsymbol{\ell}}{\partial\theta'}\frac{\partial\theta}{\partial\alpha'} \qquad (\alpha = u,v,w)
\end{aligned} \tag{2.40}$$

Equation (2.38) is valid for any arbitrary δu, δv, δw and $\delta\phi$, implying that the individual integrands be equal to zero (Török, 2000). Thus the equations and boundary conditions for the flexural-flexural-torsional vibrations of a cantilever beam are given by

$$m\ddot{u} - Q^*_u = G'_u, \quad m\ddot{v} - Q^*_v = G'_v, \quad m\ddot{w} - Q^*_w = G'_w, \quad Q^*_\phi = A_\phi$$

$$\left[-G_u\delta u - G_v\delta v - G_w\delta w + H_u\delta u' + H_v\delta v' + H_w\delta w' + \frac{\partial \ell}{\partial \phi'}\delta\phi \right]_{s=0}^{l} = 0 \tag{2.41}$$

2.7 Order Three Equations of Motion

The equations of motion derived in the previous section are simplified to include nonlinear effects up to order three. This is accomplished by expanding each term in the equations into a Taylor series and discarding terms of order greater than three. The simplification is necessary to enable the use of the equations to study the motion of the beam via numerical techniques. Previous mathematical models for the non linear vibration of cantilever beams included nonlinearities up to order two (Crespo da Silva, 1978). This model is more complete since it incorporates nonlinearities up to order three.

The simplification process begins by obtaining the order three Taylor series expansions of u', ψ, and θ. These are derived using the Taylor series expansion of *arctan(x)*

$$\tan^{-1} x = x - \frac{1}{3}x^3 + \ldots \tag{2.42}$$

which is combined with (2.10), and (2.11) to get

$$u' = [1 - (v')^2 - (w')^2]^{1/2} - 1 = -\frac{1}{2}[(v')^2 + (w')^2] + \ldots \tag{2.43}$$

$$\psi = \tan^{-1}\frac{v'}{1+u'} = \tan^{-1}\{v'[1 - (v')^2 - (w')^2]^{-1/2}\} = v'[1 + \frac{1}{6}(v')^2 + \frac{1}{2}(w')^2] + \ldots \tag{2.44}$$

$$\theta = \tan^{-1}\frac{-w'}{[(1+u')^2 + (v')^2]^{1/2}} = \tan^{-1}\{-w'[1 - (w')^2]^{-1/2}\} = -w'[1 + \frac{1}{6}(w')^2] + \ldots \tag{2.45}$$

The order three expansion for the angle of twist is obtained from the twisting curvature ρ_ξ. The third order expansion for the twisting curvature is given by

$$\rho_\xi = \phi' + v'' w' \tag{2.46}$$

Equation (2.46) is integrated over the length of the beam to obtain the order three expression for the angle of twist.

$$\gamma \equiv \phi + \int_0^s v'' w' ds \tag{2.47}$$

Expanding the remaining terms in (2.41) and retaining terms up to order three yields

$$\begin{aligned} m\ddot{u} + c_u \dot{u} - Q_u = \{ & D_\xi \gamma' (w'' v' - v'' w') - (D_\eta - D_\zeta)[w'(v''\gamma)' + v'(w''\gamma)'] \\ & + D_\zeta v''' v' + D_\eta w''' w' + \lambda(1+u') \}' \end{aligned} \tag{2.48}$$

$$\begin{aligned} m\ddot{v} + c_v \dot{v} - Q_v = \{ & -D_\xi \gamma' w''' + (D_\eta - D_\zeta)[(w''\gamma)' - (v''\gamma^2)' + w''' \int_0^s v' w'' ds \\ & - D_\zeta [v''' + v'((v'')^2 + (w'')^2)] + \lambda v' \}' \end{aligned} \tag{2.49}$$

$$\begin{aligned} m\ddot{w} + c_w \dot{w} - Q_w = \{ & D_\xi \gamma' v'' + (D_\eta - D_\zeta)[(v''\gamma)' + (w''\gamma^2)' - v''' \int_0^s w' v'' ds] \\ & - D_\eta [w''' + w'((v'')^2 + (w'')^2)] + \lambda w' \}' \end{aligned} \tag{2.50}$$

$$D_\xi \gamma'' = (D_\eta - D_\zeta)[\gamma((v'')^2 - (w'')^2) - v'' w''] \tag{2.51}$$

which are the order three equations of motion for the cantilever beam.

The boundary conditions for the fixed end are given by

$$\alpha(0,t) = 0 \qquad (\alpha = u, v, w, \gamma, v', w') \tag{2.52}$$

The natural boundary conditions obtained from (2.41-e) are used for the free end of the beam. Thus, the boundary conditions for the free end are given by

$$\alpha(l,t) = 0 \qquad (\alpha = H_v - H_u \frac{v'}{1+u'}, H_w - H_u \frac{w'}{1+u'}, \gamma') \tag{2.53}$$

$$G_\alpha(l,t) = 0 \qquad (\alpha = u, v, w) \tag{2.54}$$

Equations (2.49) and (2.50) are further simplified by removing λ and γ using the Taylor series expansions of *u,* λ and γ. The expansion of *u* is obtained directly from (2.43) as

$$u = -\frac{1}{2}\int_0^s [(v')^2 + (w')^2] ds \tag{2.55}$$

Equations (2.55), (2.47), (2.48), (2.49), and (2.50) suggest *u*, λ and γ are of order two.

Equation (2.55) is substituted into (2.48) and only terms up to order two are kept. Integrating the resulting expression from *l* to *s*, produces the expression for the Lagrange multiplier λ in terms of the transverse displacements. Incidentally, the Lagrange multiplier is interpreted as an axial force necessary to maintain the inextensionality constraint (Malatkar, 2003).

$$\lambda = -D_\zeta v'''v' - D_\eta w'''w' - \frac{1}{2} m \int_l^s \frac{\partial^2}{\partial t^2} [\int_0^s [(v')^2 + (w')^2] ds] ds - \int_l^s Q_u ds \tag{2.56}$$

For the angle of twist, (2.51) is integrated twice and only terms up to order two are retained. The angle of twist is then

$$\gamma = -\frac{D_\eta - D_\zeta}{D_\xi} \int_0^s \int_l^s v''w'' ds ds \tag{2.57}$$

Equation (2.57) indicates flexure induced torsion is a nonlinear phenomenon (Malatkar, 2003).

Substituting (2.56) and (2.57) into (2.49) and (2.50) yields the order three equations of motion for the flexural-flexural-torsional vibration of a cantilever beam.

$$\begin{aligned} m\ddot{v} + c_v\dot{v} + D_\zeta v^{iv} &= Q_v + \{(D_\eta - D_\zeta)\left[w'' \int_l^s v'' w'' ds - w''' \int_0^s v'' w' ds \right] \\ &\quad - \frac{(D_\eta - D_\zeta)^2}{D_\xi}(w'' \int_0^s \int_l^s v'' w'' ds ds)'\}' - D_\zeta\{v'(v'v'' + w'w'')'\}' \\ &\quad - \frac{1}{2}m\{v' \int_l^s \frac{\partial^2}{\partial t^2}[\int_0^s (v'^2 + w'^2)ds]ds\}' - (v' \int_l^s Q_u ds)' \end{aligned} \tag{2.58}$$

$$\begin{aligned} m\ddot{w} + c_w\dot{w} + D_\eta w^{iv} &= Q_w - \{(D_\eta - D_\zeta)\left[v'' \int_l^s v'' w'' ds - v''' \int_0^s w'' v' ds \right] \\ &\quad + \frac{(D_\eta - D_\zeta)^2}{D_\xi}(v'' \int_0^s \int_l^s v'' w'' ds ds)'\}' - D_\eta\{w'(v'v'' + w'w'')'\}' \\ &\quad - \frac{1}{2}m\{w' \int_l^s \frac{\partial^2}{\partial t^2}[\int_0^s (v'^2 + w'^2)ds]ds\}' - (w' \int_l^s Q_u ds)' \end{aligned} \tag{2.59}$$

The boundary conditions for (2.58) and (2.59) are given by

$$\begin{aligned} &v(0,t) = 0, \quad w(0,t) = 0, \quad v'(0,t) = 0, \quad w'(0,t) = 0 \\ &v''(l,t) = 0, \quad w''(l,t) = 0, \quad v'''(l,t) = 0, \quad w'''(l,t) = 0 \end{aligned} \tag{2.60}$$

The boundary conditions for the free end are derived from (2.53).

The equation of motion and boundary conditions for the forced planar flexural vibration of the beam is obtained from equations (2.58) and (2.59). For planar motion, equation (2.59) is dropped along with the *w* terms in (2.58). With these substitutions equation (2.58) becomes

$$m\ddot{v} + c_v\dot{v} + D_\zeta v^{iv} = Q_v - D_\zeta\{v'(v'v'')'\}' - \frac{1}{2}m\{v'\int_l^s \frac{\partial^2}{\partial t^2}[\int_0^s v'^2\, ds]ds\}' - (v'\int_l^s Q_u ds)' \qquad (2.61)$$

For base excitation of the vertical beam, the transverse displacement v is given by

$$v = v_b + v_0\cos(\Omega t) \qquad (2.62)$$

where v_b is the transverse displacement of the beam relative to the base, v_0 the amplitude of the excitation at the base, and Ω the excitation frequency. Moreover, the generalized force Q_v is zero and the generalized force Q_u is the weight per unit length.

$$Q_u = mg, \qquad Q_v = 0 \qquad (2.63)$$

Substituting (2.62) and (2.63) into (2.61) yields the equation for the planar flexural forced vibration of the beam

$$\begin{aligned}\rho A\ddot{v} + c_v\dot{v} + EIv^{iv} &= \rho Ag[v''(s-l) + v'] - EI\{v'(v'v'')'\}' \\ &\quad - \frac{1}{2}\rho A\{v'\int_l^s \frac{\partial^2}{\partial t^2}[\int_0^s v'^2\, ds]ds\}' + \rho A a_b\cos\Omega t\end{aligned} \qquad (2.64)$$

where ρ, A, c_v, E, I, and a_b are the density, cross sectional area, viscous damping coefficient, Young's modulus, moment of inertia and acceleration applied at the base, respectively.

The first term on the right hand side of (2.64) arises from the effect of gravity on the beam. The second and third terms represent the curvature and inertia nonlinearity, respectively.

Chapter 3: Numerical Solution

This chapter develops the numerical algorithm used to solve the equation of motion for the planar flexural forced vibration of the cantilever beam (2.64). The partial differential equation is first discretized in the spatial coordinate using Galerkin's weighted residual method (Section 3.1). Then, the equation is discretized in the time domain using the Newmark technique (Section 3.2). Finally, a numerical algorithm is used to calculate the nonlinear response of the beam (Section 3.3).

3.1 Finite Element Model

The equation of motion for the nonlinear planar flexural forced vibration of a cantilever beam was derived in the previous chapter. The equation of motion for the transverse displacement in the *y* direction is given by

$$\begin{aligned}\rho A\ddot{v} + c_v\dot{v} + EIv^{iv} &= \rho Ag[v''(s-l)+v'] - EI\{v'(v'v'')'\}' \\ &\quad -\frac{1}{2}\rho A\{v'\int_l^s \frac{\partial^2}{\partial t^2}[\int_0^s v'^2\, ds]ds\}' + \rho Aa_b\cos\Omega t\end{aligned} \tag{3.1}$$

This equation can be written in the form

$$\rho A\ddot{v} + c_v\dot{v} + EIv^{iv} - \rho Agf_3 + EI\{v'f_1\}' + \frac{1}{2}\rho A\{v'f_2\}' - F = 0 \tag{3.2}$$

with the functions f_1, f_2, f_3 , and F given by

$$f_1 = (v'v'')', \quad f_2 = \frac{\partial^2}{\partial t^2}\int_l^s\int_0^s v'^2\, dsds, \quad f_3 = (s-l)v''+v', \quad F = \rho Aa_b\cos\Omega t \tag{3.3}$$

The functions f_1, f_2, and f_3 originate from the curvature, inertial, and gravitational nonlinear effects, respectively. The function F is the force associated with the transverse displacement exciting the base of the beam.

Equation (3.2) is a nonlinear integro-differential equation, for which a closed form solution is not available. Therefore, an approximate solution is sought by discretizing (3.2), first in the spatial coordinate using Galerkin's weighted residuals method, and then in the time domain using the Newmark technique.

The discretization in the spatial coordinate is carried out in three steps: (1) mesh generation and function approximation, (2) element equation, and (3) assembly and implementation of boundary conditions. These steps are discussed in detail in the remaining of this section. The discretization in the time domain is the focus of section 3.2.

3.1.1 Mesh Generation and Function Approximation

Figure 3.1 shows the cantilever beam divided into N cubic Hermite elements, each of length h.

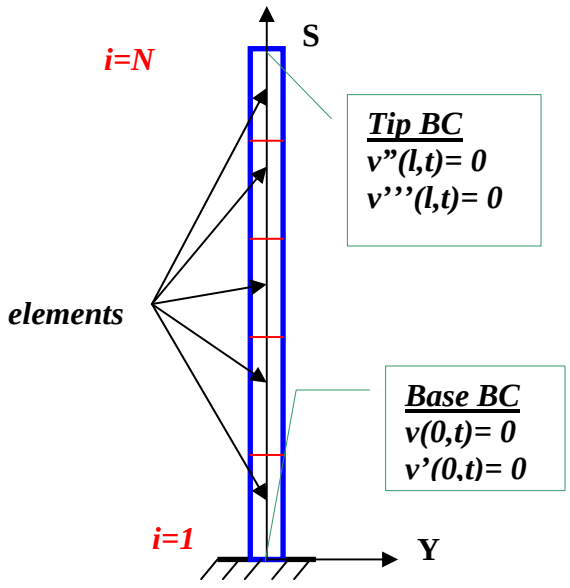

Figure 3. 1: Cantilever beam divided into N elements

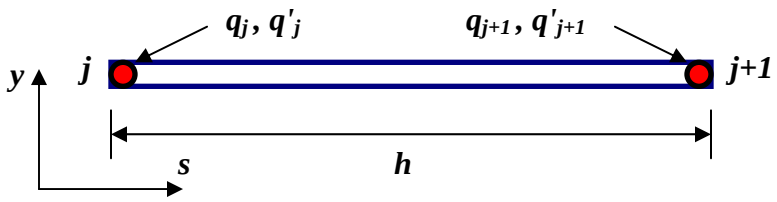

Figure 3. 2: Typical cubic Hermite beam element

The typical cubic Hermite element (Figure 3.2) has two nodes with two degrees of freedom per node (Zienkiewicz, 1977), namely translation (q_j) and slope (q'_j). The displacement of any point inside the element is approximated as

$$\tilde{v}^e(s,t) = \sum_{j=1}^{4} \psi_j(s) q_j^e(t) \tag{3.4}$$

The shape functions $\psi_j(s)$ are given by (Reddy, 1993).

$$\psi_1 = 1 - 3\left(\frac{s}{h}\right)^2 + 2\left(\frac{s}{h}\right)^3, \quad \psi_2 = h\left[\left(\frac{s}{h}\right) - 2\left(\frac{s}{h}\right)^2 + \left(\frac{s}{h}\right)^3\right],$$
$$\psi_3 = 3\left(\frac{s}{h}\right)^2 - 2\left(\frac{s}{h}\right)^3, \quad \psi_4 = h\left[-\left(\frac{s}{h}\right)^2 + \left(\frac{s}{h}\right)^3\right] \tag{3.5}$$

The vector q_j^e in (3.4) is the element nodal displacement vector. For the remaining of this derivation, the superscript e is dropped for the sake of simplicity. The numerical solution of the partial differential equation in (3.2) is a piecewise cubic polynomial comprised of the sum of the approximated displacement $\tilde{v}^e(s,t)$, i.e., $v \cong \sum_e \tilde{v}^e$.

3.1.2 Element Equation

In order to obtain the element equation, the approximated displacement in (3.4) is substituted into the partial differential equation (3.2). When this is done, the left hand side is no longer equal to zero, but to a quantity R_x called the residual.

$$\begin{aligned}\rho A\sum_{j=1}^{4}\psi_j\ddot{q}_j + c_v\sum_{j=1}^{4}\psi_j\dot{q}_j + EI\sum_{j=1}^{4}\psi_j^{iv}q_j - F - \rho Agf_3 \\ + EI[(\sum_{j=1}^{4}\psi'_j\, q_j)\, f_1]' + \frac{1}{2}\rho A[(\sum_{j=1}^{4}\psi'_j\, q_j)\, f_2]' = R_x\end{aligned} \tag{3.6}$$

The weighted residual *WR* is defined using Galerkin's method. In Galerkin's method, the shape function ψ_i is used as the weighting function. The weighted residual is forced to be zero over the element. Therefore *WR* is given by

$$WR = \int_0^h \psi_i R_x ds = 0 \tag{3.7}$$

Multiplying both sides of (3.6) by the shape function ψ_i and integrating over the length of the element results in

$$\begin{aligned}[\rho A\sum_{j=1}^{4}\int_0^h \psi_i\psi_j ds]\ddot{q}_j + [c_v\sum_{j=1}^{4}\int_0^h \psi_i\psi_j ds]\dot{q}_j + [EI\sum_{j=1}^{4}\int_0^h \psi_i\psi_j^{iv} ds]q_j - \int_0^h \psi_i F ds \\ - \rho Ag\int_0^h \psi_i f_3 ds + EI\int_0^h \psi_i[(\sum_{j=1}^{4}\psi'_j q_j)\, f_1]' ds + \frac{1}{2}\rho A\int_0^h \psi_i[(\sum_{j=1}^{4}\psi'_j q_j)\, f_2]' ds = 0\end{aligned} \tag{3.8}$$

Finally, several terms in equation (3.8) are integrated by parts to obtain the weak form of the element equation

$$[\rho A\sum_j \int_0^h \psi_i\psi_j ds]\ddot{q}_j + [c_v \sum_j \int_0^h \psi_i\psi_j ds]\dot{q}_j + [EI\sum_j \int_0^h \psi_i"\psi_j" ds]q_j - \int_0^h \psi_i F ds$$
$$- \rho Ag\int_0^h \psi_i f_3 ds - [EI\sum_j \int_0^h \psi_i'\psi_j' f_1 ds]q_j - [\frac{1}{2}\rho A\sum_j \int_0^h \psi_i'\psi_j' f_2 ds]q_j \qquad (3.9)$$
$$+ [\psi_i \sum_j \psi_j' q_j EIf_1]_0^h + [\psi_i \sum_j \psi_j' q_j f_2]_0^h + [\psi_i EI\sum_j \psi_j"' q_j - \psi_i' EI\sum_j \psi_j" q_j]_0^h = 0$$

which can be simplified to

$$M_{ij}^e \ddot{q}_j + c_{ij}^e \dot{q}_j + K_{ij}^e q_j - kc_{ij}^e q_j - ki_{ij}^e q_j - F_i^e - g_i^e + b_i^e = 0 \qquad (3.10)$$

with the matrices, M_{ij}^e , c_{ij}^e, and K_{ij}^e given by

$$M_{ij}^e = \rho A\int_0^h \psi_i\psi_j ds, \quad c_{ij}^e = c_v\int_0^h \psi_i\psi_j ds, \quad K_{ij}^e = EI\int_0^h \psi"_i\psi"_j ds \qquad (3.11)$$

These matrices are the element mass, damping and stiffness matrices, respectively. Equation (3.10) is written in indicial notation. Therefore, repeated indices denote summation.

At this point it is convenient to introduce the matrix naming convention used in the remaining of the chapter. Matrices in capital letters are linear matrices, while matrices in lower case letters are nonlinear matrices. For instance, in (3.11) the matrices M_{ij}^e and, K_{ij}^e are linear matrices, while the matrix c_{ij}^e is a nonlinear matrix.

For a cubic Hermite beam element the matrices M_{ij}^e and, K_{ij}^e are given by (Reddy, 1993)

$$M_{ij}^{e} = \frac{\rho A h}{420}\begin{bmatrix} 156 & 22h & 54 & -13h \\ 22h & 4h^2 & 13h & -3h^2 \\ 54 & 13h & 156 & -22h \\ -13h & -3h^2 & -22h & 4h^2 \end{bmatrix} \tag{3.12}$$

$$K_{ij}^{e} = \frac{EI}{h^3}\begin{bmatrix} 12 & 6h & -12 & 6h \\ 6h & 4h^2 & -6h & 2h^2 \\ -12 & -6h & 12h & -6h \\ 6h & 2h^2 & -6h & 4h^2 \end{bmatrix} \tag{3.13}$$

where ρ, A, E, I, and h are the density, cross sectional area, Young's modulus, area moment of inertia and length of the element, respectively.

Equation (3.10) has two additional stiffness matrices kc_{ij}^{e}, and ki_{ij}^{e}, resulting from the nonlinear effects in (3.2). These matrices are given by

$$kc_{ij}^{e} = EI\int_0^h \psi'_i \psi'_j f_1 \, ds \ , \qquad ki_{ij}^{e} = \frac{1}{2}\rho A\int_0^h \psi'_i \psi'_j f_2 \, ds \tag{3.14}$$

The matrix kc_{ij}^{e} represents the curvature nonlinearity, while ki_{ij}^{e} represents the inertia nonlinearity.

The vectors F_i^e and g_i^e are the force and gravitational effect vectors, respectively and are defined as

$$F_i^e = \int_0^h \psi_i F ds \ , \quad g_i^e = \rho A g\int_0^h \psi_i f_3 ds \tag{3.15}$$

The vector b_i^e is the combination of the boundary terms in (3.9).

$$b_i^e = \ [\psi_i v'(v'\boldsymbol{\mathcal{V}} + v''\boldsymbol{\mathcal{M}})]_0^h + [\psi_i v'\boldsymbol{\mathcal{F}}_{\boldsymbol{\alpha}}]_0^h + [\psi_i \boldsymbol{\mathcal{V}} - \psi_i{}'\boldsymbol{\mathcal{M}}]_0^h \tag{3.16}$$

The quantities $\mathcal{V}$ and $\mathcal{M}$ in (3.16) are the transverse shear force and bending moment of the beam. For a beam, the bending moment and shear force are given by (Rao, 1990)

$$\mathcal{M} = EIv'' \ , \quad \mathcal{V} = (EIv'')' \tag{3.17}$$

The force $\mathcal{F}_a$ in (3.16) can be interpreted as part of the axial force required to maintain the inextensionality constraint. The origin of $\mathcal{F}_a$ is understood upon examination of the order two expression for the Lagrange multiplier derived in the previous chapter.

The Lagrange multiplier is interpreted as the axial force required to maintain the inextensionality constraint (Malatkar, 2003). Recall from Chapter 2, the order two expression for the Lagrange multiplier is

$$\lambda = -D_\varsigma v'''v' - D_\eta w'''w' - \frac{1}{2} m \int_l^s \frac{\partial^2}{\partial t^2} [\int_0^s [(v')^2 + (w')^2] ds] ds - \int_l^s Q_u ds \tag{3.18}$$

For planar motion of the cantilever beam (3.18) becomes

$$\lambda = -EIv'''v' - \frac{1}{2} \rho A \int_l^s \frac{\partial^2}{\partial t^2} [\int_0^s v'^2 \, ds] ds - \rho A g (s - l) \tag{3.19}$$

which can be written as

$$\lambda = -\mathcal{F}_e - \mathcal{F}_a - \mathcal{W}_\ell \tag{3.20}$$

with $\mathcal{F}_e$, $\mathcal{F}_a$, and $\mathcal{W}_\ell$ given by

$$\mathcal{F}_e = EIv'''v' \ , \quad \mathcal{F}_a = \frac{1}{2} \rho A \int_l^s \frac{\partial^2}{\partial t^2} [\int_0^s v'^2 \, ds] ds \ , \quad \mathcal{W}_\ell = \rho A g (s - l) \tag{3.21}$$

From (3.20) it is clear the Lagrange multiplier λ is the combination of three forces, namely the elastic force *($\mathcal{F}_e$),* the inertial force *($\mathcal{F}_a$)* and the weight of the beam above point *s* along the neutral axis *($\mathcal{W}_s$)*. Hence, $\mathcal{F}_a$ is indeed part of the axial force required to maintain the inextensionality constraint.

3.1.3 Assembly and Implementation of Boundary Conditions

Assembly of the *N* element equations yields the global finite element equation

$$M_{ij}\ddot{q}_j + c_{ij}\dot{q}_j + k_{ij}q_j = f_i + b_i \tag{3.22}$$

which is a system of *2(N+1)* ordinary differential equations, i.e., one for each nodal degree of freedom. The solution of this system is the vector q_j, which contains the nodal displacements and nodal rotations in the global coordinates *S* and *Y* (Figure 3.1). The global linear mass matrix M_{ij} is calculated using (3.12).

The nonlinear damping matrix c_{ij} is calculated using proportional damping (Cook, 1995). Therefore, c_{ij} is approximated as a linear combination of the mass and nonlinear stiffness matrices.

$$c_{ij} = \alpha_1 M_{ij} + \alpha_2 k_{ij} \tag{3.23}$$

The coefficients α_1 and α_2 are calculated using the natural frequencies and modal damping ratios of the system. The procedure to calculate these coefficients is discussed in detail in section 3.3.

The nonlinear stiffness matrix k_{ij} is the combination of the linear stiffness matrix, calculated using (3.13), and the two nonlinear stiffness matrices kc_{ij} and ki_{ij}, calculated with (3.14).

$$k_{ij} = K_{ij} - kc_{ij} - ki_{ij} \tag{3.24}$$

The nonlinear force vector f_i is the combination of the linear force vector and the gravitational effect vector, both calculated with (3.15).

$$f_i = F_i + g_i \tag{3.25}$$

The boundary vector b_i is defined using the element boundary vector given by (3.16). The internal reactions $\boldsymbol{V}$, $\boldsymbol{M}$, and $\boldsymbol{F_a}$ in (3.16) cancel out upon assembly for all nodes except for the first and last nodes. Therefore, the global boundary vector has non zero elements only at the fixed and free ends of the beam. The boundary conditions of the problem are used to evaluate b_i. From the previous chapter the boundary conditions are

$$\begin{aligned} v(0,t) &= 0, & v'(0,t) &= 0 \\ v''(l,t) &= 0, & v'''(l,t) &= 0 \end{aligned} \tag{3.26}$$

The elements of the boundary vector for the fixed end are given by

$$\begin{aligned} b_1 &= \psi_1 v'(v'\boldsymbol{V} + v''\boldsymbol{M}) + \psi_1 v'\boldsymbol{F_a} + \psi_1 \boldsymbol{V} - \psi_1' \boldsymbol{M} \\ b_2 &= \psi_2 v'(v'\boldsymbol{V} + v''\boldsymbol{M}) + \psi_2 v'\boldsymbol{F_a} + \psi_2 \boldsymbol{V} - \psi_2' \boldsymbol{M} \end{aligned} \tag{3.27}$$

For the fixed end, v' is zero according to the boundary conditions in (3.26). Therefore, the first two terms of b_1 and b_2 vanish and (3.27) becomes

$$b_1 = \psi_1 \boldsymbol{V} - \psi_1' \boldsymbol{M} \ , \qquad b_2 = \psi_2 \boldsymbol{V} - \psi_2' \boldsymbol{M} \tag{3.28}$$

The elements of the boundary vector corresponding to the free end are

$$\begin{aligned} b_{2(N+1)-1} &= \psi_3 v'(v'\mathcal{V} + v''\mathcal{M}) - \psi_3'\mathcal{M} + \psi_3\mathcal{V} + \psi_3 v'\mathcal{F}_a \\ b_{2(N+1)} &= \psi_4 v'(v'\mathcal{V} + v''\mathcal{M}) - \psi_4'\mathcal{M} + \psi_4\mathcal{V} + \psi_4 v'\mathcal{F}_a \end{aligned} \tag{3.29}$$

For the free end, both v'' and v''' are zero from the boundary conditions. As a result, both the shear force and bending moment are zero according to (3.17), causing the first three terms in (3.29) to vanish. Also, the inertial force $\mathcal{F}_a$ is zero at the free end, according to (3.21). Therefore, both $b_{2(N+1)-1}$ and $b_{2(N+1)}$ are zero.

$$b_{2(N+1)-1} = b_{2(N+1)} = 0 \tag{3.30}$$

Since the displacement and rotation at the fixed end are both known from the boundary conditions, the first two equations in (3.22) do not need to be included as part of the system of equations to be solved. These equations are saved for post processing of the solution.

Substituting the boundary vector b_i into (3.22), and saving the first two equations of the system for post processing yields

$$M_{ij}^r \ddot{q}_j + c_{ij}^r \dot{q}_j + k_{ij}^r q_j = f_i^r \tag{3.31}$$

The superscript r in (3.31) stands for reduced, since the first two equations are eliminated.

3.2 Newmark Technique

In this section, the linear global finite element equation of motion is used to illustrate the Newmark technique. The linear equation of motion is given by

$$M_{ij}\ddot{Q}_j + C_{ij}\dot{Q}_j + K_{ij}Q_j = F_i \tag{3.32}$$

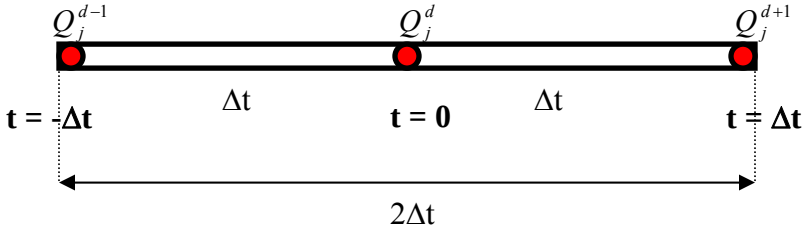

Figure 3. 3: Interval for discretization in the time domain

and is obtained by omitting the nonlinear matrices kc_{ij} and ki_{ij}, as well as the gravitational effect vector g_i in (3.31). The matrices M_{ij}, C_{ij}, K_{ij} and the vector F_i are reduced matrices since the first two rows and columns are eliminated. However, the superscript *r* is dropped for simplicity.

Equation (3.32) is discretized within the time interval [-Δt,Δt], where Δt is the time step (Figure 3.3) and *t* is an arbitrary time. This interval is divided in two segments of length Δt each. Dividing the interval in this manner creates three discrete time points (Figure 3). For each one of these *time nodes*[5] there is a displacement vector associated to it. The displacement vector for time Δt is Q_j^{d+1}, while the displacement vectors for times *0* and -Δt are Q_j^{d} and Q_j^{d-1}, respectively.

The displacement vector at any time inside the interval in Figure 3.3 is approximated by[6]

$$Q_j = \Phi_{d-1}Q_j^{d-1} + \Phi_d Q_j^{d} + \Phi_{d+1}Q_j^{d+1} = \Phi_k Q_j^{k} \tag{3.33}$$

where Φ_{d-1}, Φ_d, and Φ_{d+1} are the shape functions given by (Zienkiewicz, 1977)

[5] Nodes in the time interval are called time nodes from now on, to avoid confusion with the nodes used for the discretization in the spatial coordinate (section 3.1).
[6] Equation (3.33) is written in indicial notation. Therefore, repeated indices denote summation.

$$\Phi_{d-1} = \frac{-\nu}{2}(1-\nu)\,,\quad \Phi_d = (1-\nu)(1+\nu)\,,\quad \Phi_{d+1} = \frac{\nu}{2}(1+\nu) \tag{3.34}$$

The dimensionless time coordinate ν in (3.34) is defined as

$$\nu = \frac{t}{\Delta t} \tag{3.35}$$

The displacement vector Q_j in (3.33) is a quadratic polynomial in *t*. The force inside the interval [-Δt, Δt] is interpolated in a way similar to the displacement vector (Zienkiewicz, 1977). Therefore the force F_i is given by

$$F_i = \Phi_{d-1} F_i^{d-1} + \Phi_d F_i^d + \Phi_{d+1} F_i^{d+1} = \Phi_k F_i^k \tag{3.36}$$

Substitution of (3.33) and (3.36) into (3.32) yields the residual R_t.

$$M_{ij}\ddot{\Phi}_k Q_j^k + C_{ij}\dot{\Phi}_k Q_j^k + K_{ij}\Phi_k Q_j^k - \Phi_k F_i^k = R_t \tag{3.37}$$

with *k* ranging from *d-1* to *d+1*. The weighted residual method is applied by multiplying (3.37) by a weighting function *ω(t)* and integrating from *-Δt* to *Δt*. Equation (3.37) becomes then

$$\int_{-\Delta t}^{\Delta t} \omega(t)[M_{ij}\ddot{\Phi}_k Q_j^k + C_{ij}\dot{\Phi}_k Q_j^k + K_{ij}\Phi_k Q_j^k - \Phi_k F_i^k]dt = 0 \tag{3.38}$$

Substituting the shape functions (3.34) into (3.38) results in

$$\begin{aligned} &\{M_{ij} + \gamma\Delta t C_{ij} + \beta\Delta t^2 K_{ij}\}Q_j^{d+1} + \{-2M_{ij} + (1-2\gamma)\Delta t C_{ij} \\ &+ (0.5-2\beta+\gamma)\Delta t^2 K_{ij}\}Q_j^d + \{M_{ij} - (1-\gamma)\Delta t C_{ij} + (0.5+\beta-\gamma)\Delta t^2 K_{ij}\}Q_j^{d-1} \\ &- \Delta t^2\{\beta F_i^{d+1} + (0.5-2\beta+\gamma)F_i^d + (0.5+\beta-\gamma)F_i^{d-1}\} = 0 \end{aligned} \tag{3.39}$$

where the quantities γ and β are given by

$$\gamma = \frac{\int_{-1}^{1} \omega(\nu)(\nu + \frac{1}{2}) d\nu}{\int_{-1}^{1} \omega(\nu) d\nu}, \quad \beta = \frac{\frac{1}{2}\int_{-1}^{1} \omega(\nu)(1+\nu)\nu d\nu}{\int_{-1}^{1} \omega(\nu) d\nu} \tag{3.40}$$

Notice the variable of integration in (3.40) has been changed from *t* to the dimensionless time coordinate ν (3.35).

Equation (3.39) can be simplified to

$$A1_{ij} Q_j^{d+1} + A2_{ij} Q_j^d + A3_{ij} Q_j^{d-1} - \mathcal{F}_i = 0 \tag{3.41}$$

where the matrices $A1_{ij}$, $A2_{ij}$, $A3_{ij}$ and the vector $\mathcal{F}_i$ are defined as follows

$$\begin{aligned} A1_{ij} &= M_{ij} + \gamma \Delta t C_{ij} + \beta \Delta t^2 K_{ij} \\ A2_{ij} &= -2M_{ij} + (1-2\gamma)\Delta t C_{ij} + (0.5 - 2\beta + \gamma)\Delta t^2 K_{ij} \\ A3_{ij} &= M_{ij} - (1-\gamma)\Delta t C_{ij} + (0.5 + \beta - \gamma)\Delta t^2 K_{ij} \end{aligned} \tag{3.42}$$

$$\mathcal{F}_i = \Delta t^2 \{\beta F_i^{d+1} + (0.5 - 2\beta + \gamma) F_i^d + (0.5 + \beta - \gamma) F_i^{d-1}\} \tag{3.43}$$

Equation (3.41) is used to solve for the displacement vector Q_j^{d+1} in terms of the displacement vectors Q_j^d and Q_j^{d-1}.

$$Q_j^{d+1} = A1_{ij}^{-1`} A2_{il} Q_l^d - A1_{ij}^{-1} A3_{il} Q_l^{d-1} + \Delta t^2 A1_{ij}^{-1} \mathcal{F}_i \tag{3.44}$$

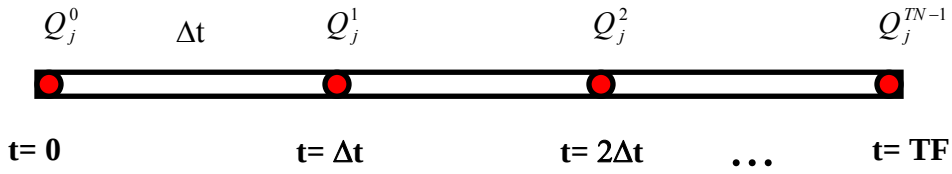

Figure 3. 4: Time nodes in [0,TF]

The use of (3.44) to calculate the time history of the displacement vector Q_j in the interval [0,TF] is illustrated next. Here *TF* is an arbitrary time. The time interval [0,TF] has *TN* time nodes with *TN* given by (Figure 3.4)

$$TN = \frac{TF}{\Delta t} + 1 \tag{3.45}$$

The first time node corresponds to *d=1*, the second to *d=2,* and so on.

The displacement vector for the second time node in [0,TF] is simply Q_j^1. In order to calculate Q_j^1, the vectors Q_j^0 and Q_j^{-1} must be prescribed. This is done by using the initial conditions of the problem. For this problem it is assumed the beam starts from rest, which means the displacement vectors Q_j^0 and Q_j^{-1} are equal to the zero vector.

$$Q_j^0 = Q_j^{-1} = 0 \tag{3.46}$$

Substituting *d=0* along with (3.46) into (3.44) yields

$$Q_j^1 = \Delta t^2 A1_{ij}^{-1} \mathcal{F}_i$$

(3.47)

The force vector $\mathcal{F}_i$ is given by (3.43). The vectors Q_j^0 and Q_j^1 are substituted in (3.44) to calculate Q_j^2, the displacement vector for the next time node. In this manner (3.44) is used to calculate the displacement vectors for all time nodes in [0,TF].

The quantities γ and β in (3.40) vary depending on the choice for weighting function $\omega(v)$. For this problem, the values γ = 0.5 and β = 0.25 are used. This corresponds to an average acceleration scheme (Zienkiewicz, 1977). These values of γ and β ensure the computation of the time history of the displacement vector using (3.44) is unconditionally stable, i.e., independent of the size of Δt (Bathe, 1973).

3.3 Numerical Algorithm

Figure 3.5 illustrates the process used to calculate the time history of the nonlinear displacement vector q_j.

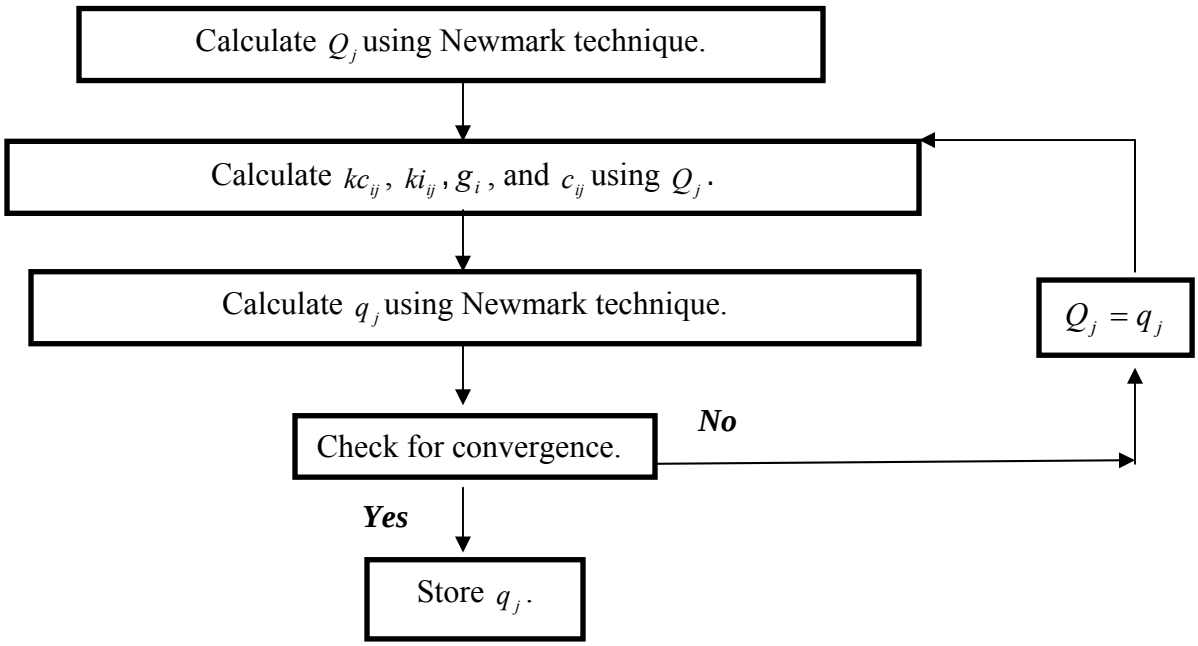

Figure 3. 5: Algorithm used to calculate the time history of the displacement

The linear displacement vector Q_j is calculated first. This linear displacement vector is then used to calculate a first guess of q_j. Finally, the iterative process is used to obtain

the nonlinear displacement vector q_j for time *t*. This algorithm is implemented in the Matlab® program *NLB*[7] in Appendix A.

3.3.1 Calculation of the Linear Displacement Q_j

The Newmark technique is used to calculate the linear displacement vector Q_j in the interval [0,TF], with $0 < t < TF$. This interval is divided in *TN* time nodes with *TN* defined by (3.45).

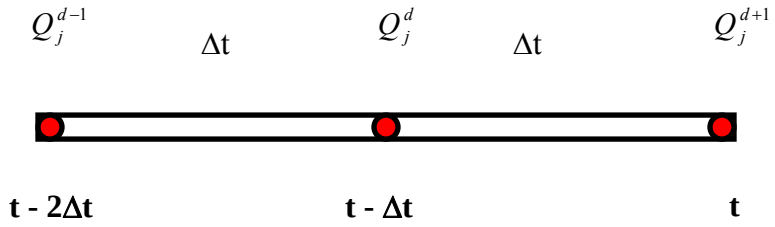

Figure 3. 6: Displacement vectors used to calculate Q_j at time t

The linear displacement vector at time *t* is given by

$$Q_j^{d+1} = A1_{ij}^{-1`} A2_{il} Q_l^d - A1_{ij}^{-1} A3_{il} Q_l^{d-1} + \Delta t^2 A1_{ij}^{-1} \mathcal{F}_i \tag{3.48}$$

where Q_j^d, Q_j^{d-1} are the linear displacement vectors for times $t - \Delta t$, and $t - 2\Delta t$, respectively (Figure 3.6).

The matrices $A1_{ij}$, $A2_{ij}$, and $A3_{ij}$ are calculated using the global linear mass and stiffness matrices.

[7] Non Linear Beam

$$
\begin{aligned}
A1_{ij} &= M_{ij} + \gamma \Delta t C_{ij} + \beta \Delta t^2 K_{ij} \\
A2_{ij} &= -2M_{ij} + (1-2\gamma)\Delta t C_{ij} + (0.5 - 2\beta + \gamma)\Delta t^2 K_{ij} \\
A3_{ij} &= M_{ij} - (1-\gamma)\Delta t C_{ij} + (0.5 + \beta - \gamma)\Delta t^2 K_{ij}
\end{aligned}
\tag{3.49}
$$

The coefficients γ and β are taken as 0.5 and 0.25, respectively. This corresponds to the average acceleration scheme (Zienkiewicz, 1977).

The matrix C_{ij} is the linear damping matrix and is calculated as a linear combination of the mass and stiffness matrices (Cook, 1995). Thus C_{ij} is given by

$$
C_{ij} = \alpha_1 M_{ij} + \alpha_2 K_{ij} \tag{3.50}
$$

The coefficients α_1 and α_2 are obtained by solving the system

$$
\xi_1 = \frac{\alpha_1}{2\omega_1} + \frac{\alpha_2 \omega_1}{2}, \qquad \xi_4 = \frac{\alpha_1}{2\omega_4} + \frac{\alpha_2 \omega_4}{2} \tag{3.51}
$$

The focus of this investigation is the time response of the cantilever beam when the base is excited at a frequency close to the third natural frequency. Therefore, the first and fourth natural frequencies and modal damping ratios are used in (3.51).

The force vector in (3.48) is calculated as

$$
\mathcal{F}_i = \Delta t^2 \{\beta F_i^{d+1} + (0.5 - 2\beta + \gamma) F_i^d + (0.5 + \beta - \gamma) F_i^{d-1}\} \tag{3.52}
$$

where F_i^{d+1}, F_i^d , and F_i^{d-1} are the linear force vectors for times *t*, *t* - Δt, and *t* - $2\Delta t$, respectively (Figure 3.6).

3.3.1 Calculation of the Nonlinear Displacement q_j

The nonlinear displacement vector at an arbitrary time *t* in [0,TF] is given by

$$q_j^{d+1} = a1_{ij}^{-1} a2_{il} q_l^d - a1_{ij}^{-1} a3_{il} q_l^{d-1} + \Delta t^2 a1_{ij}^{-1} f_l \qquad (3.53)$$

where q_j^d, q_j^{d-1} are the nonlinear displacement vectors for times $t - \Delta t$, and $t - 2\Delta t$, respectively (Figure 3.8).

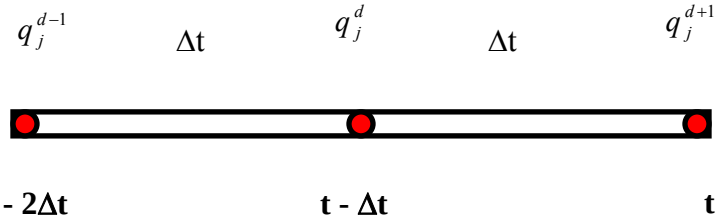

Figure 3. 7: Displacement vectors used to calculate q_j at time t

The matrices $a1_{ij}$, $a2_{ij}$ and $a3_{ij}$ in (3.53) are calculated using the global linear mass matrix and the nonlinear stiffness matrix k_{ij} given by (3.24).

$$\begin{aligned} a1_{ij} &= M_{ij} + \gamma \Delta t c_{ij} + \beta \Delta t^2 k_{ij} \\ a2_{ij} &= -2M_{ij} + (1-2\gamma)\Delta t c_{ij} + (0.5 - 2\beta + \gamma)\Delta t^2 k_{ij} \\ a3_{ij} &= M_{ij} - (1-\gamma)\Delta t c_{ij} + (0.5 + \beta - \gamma)\Delta t^2 k_{ij} \end{aligned} \qquad (3.54)$$

The coefficients γ and β are taken as 0.5 and 0.25, respectively. This corresponds to the average acceleration scheme (Zienkiewicz, 1977).

In order to obtain the nonlinear stiffness matrix k_{ij}, the functions f_1 and f_2 defined in (3.3-a) and (3.3-b) must be calculated. These functions are used with (3.14) to compute the nonlinear stiffness matrices kc_{ij} and ki_{ij}, which are substituted into (3.24) to

obtain k_{ij}. A detailed example of the procedure used to calculate ki_{ij} is included in Appendix D. The matrix kc_{ij} is calculated using a similar procedure.

The matrix c_{ij} is the nonlinear damping matrix and is calculated as a linear combination of the mass and stiffness matrices (Cook, 1995).

$$c_{ij} = \alpha_1 M_{ij} + \alpha_2 k_{ij} \tag{3.55}$$

The coeffiecients α_1 and α_2 are the same as in section 3.3.1.

The force vector in (3.53) is calculated as

$$f_i = \Delta t^2 \{\beta f_i^{d+1} + (0.5 - 2\beta + \gamma) f_i^d + (0.5 + \beta - \gamma) f_i^{d-1}\} \tag{3.56}$$

where f_i^{d+1}, f_i^d, and f_i^{d-1} are the nonlinear force vectors for times *t*, *t* - Δt, and *t* - $2\Delta t$, respectively (Figure 3.7).

The nonlinear force vector f_i is simply the combination of the linear force vector and the gravitational effect vector (3.25). The gravitational effect vector is calculated using a procedure similar to the one illustrated in Appendix D.

3.3.3 Iterative Procedure

The iterative procedure used to obtain the nonlinear displacement vector at any given time *t* is illustrated in Figure 3.5. Once vectors Q_j and q_j are obtained as discussed in sections 3.3.1 and 3.3.2, the error θ is calculated

$$\theta = \sum_{m=1}^{k} \left| q_j^m - Q_j^m \right|$$

$$\theta \le TOL \quad for\ convergence \tag{3.57}$$

where k is the total number of elements in each vector.

The error θ is compared to a maximum allowed error TOL. Once $\theta \le TOL$, the solution is converged and the vector q_j is stored. However, if the error θ exceeds the maximum allowed error, q_j is assigned to Q_j and a new q_j is calculated (Figure 3.5). This procedure is repeated until convergence is achieved.

Chapter 4: Time Response

This chapter is devoted to the study of the time response of the cantilever beam. The experimental results, obtained by Malatkar (2003), for the steady state response of the beam are presented first. These experimental results are compared with the corresponding numerical results, obtained with the *NLB*[8] program in Appendix A. Then the *NLB* program is used to calculate the transient response of the beam, which is compared against results from a finite element model developed in ANSYS®.

4.1 Experimental Steady State Response

Figure 4.1 shows the experimental set up used by Malatkar (2003) to measure the time response of the cantilever beam when subjected to harmonic excitation at the base. The beam is made of steel with Young's modulus of *165.5 GPa*, density of *7400 kg/m*^{3} and dimensions as indicated in Figure 4.1.

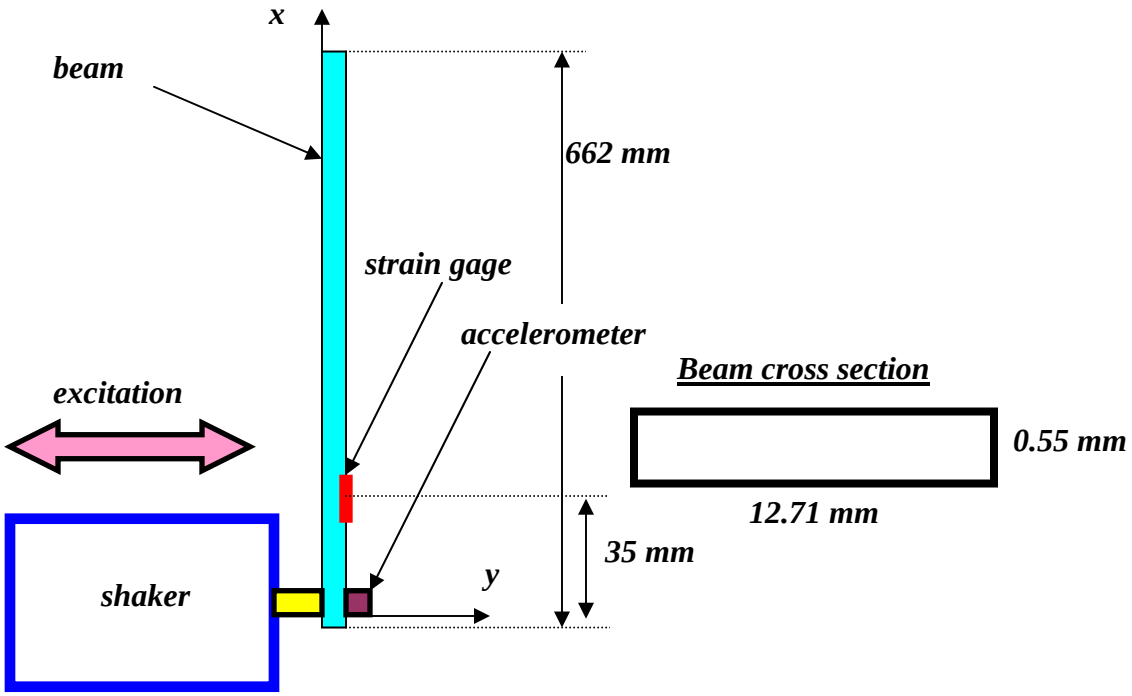

Figure 4. 1: Experimental set up

[8] Non Linear Beam

The shaker excites the base of the beam in the *y* direction (Figure 4.1). An accelerometer is attached at the same point to monitor the input excitation to the beam. A strain gage is mounted approximately *35 mm* from the base. At this location the strains are maximum and also easy to measure. The strain read at the base is used to obtain the frequency response.

The harmonic excitation applied by the shaker to the base of the beam is given by

$$F = \rho A a_b \cos \Omega t \tag{4.1}$$

where ρ, A, a_b, and Ω are the density, cross sectional area, maximum amplitude of acceleration at the base, and excitation frequency, respectively. Malatkar (2003) used an excitation frequency of *17.547 Hz* with a maximum amplitude of acceleration equal to *2.97g*, where *g* is the acceleration due to gravity. Transients were allowed to die out before the response was recorded.

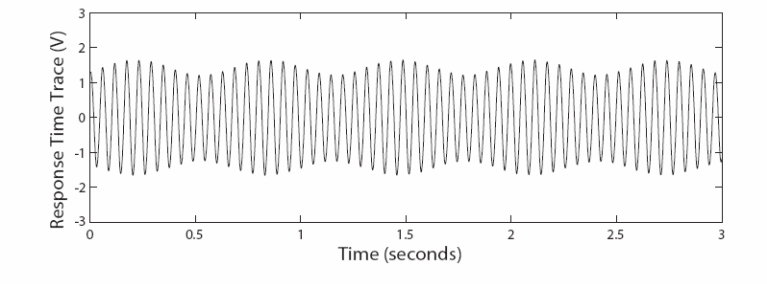

Figure 4. 2: Time response for Ω= 17.547 Hz, a_b= 2.97g

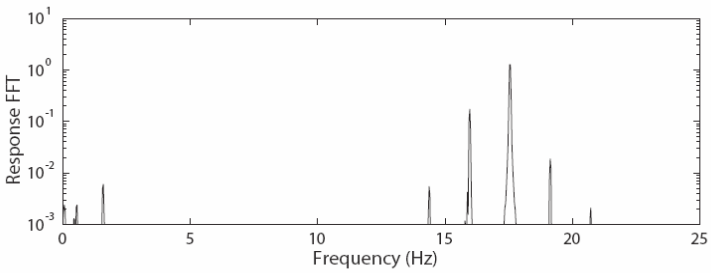

Figure 4. 3: FFT for Ω= 17.547 Hz, a_b= 2.97g

Figure 4.2 shows the time response of the vertical cantilever beam (Figure 4.1) when $\Omega = 17.547\ Hz$ and $a_b = 2.97g$. This excitation frequency is close to the third natural frequency of the beam (Table 4.1). The time response of the beam consists of a high frequency component modulated by a low frequency component.

Table 4. 1: Experimental natural frequencies and damping ratios[9]

Mode number (n)	$f_n(Hz)$	ξ_n
1	0.574	0.009
2	5.727	0.00185
3	16.55	0.00225
4	32.67	0.005

The response in Figure 4.2 is not the actual displacement, but the strain reading in Volts. However, the frequency response obtained with the strain reading will be the same as the frequency response obtained using the actual displacement. Hence, the strain results can be used to determine the frequency response of the beam at the base.

The FFT shown in Figure 4.3 is used to determine the actual frequency components present in the time trace (Figure 4.2). The high frequency component is centered at *17.547 Hz*, i.e., the excitation frequency. The asymmetric sideband structure around the high frequency peak indicates the third mode frequency component is modulated (Malatkar, 2003). The modulation frequency can be calculated from the sideband spacing, and it is found to be *1.58 Hz* for this case.

Figure 4.3 also indicates the presence of a low frequency component in the response. This low frequency component is centered at *1.58 Hz*, i.e., the modulation frequency of the high frequency component. Anderson, et al. (1992) found the low frequency component in the response of a beam excited close to a high frequency mode, is equal to the modulation frequency of the high frequency component.

[9] Natural frequencies measured by Malatkar (2003) for the vertical beam. The natural frequencies are lower than for a horizontal beam (Table B.1) due to the effect of gravity (Blevins, 1979).

4.2 Numerical Steady State Response

The numerical results for the response of a point at the base of the beam are presented next. The results were obtained with the program *NLB*, included in Appendix A. The beam dimensions and material properties used are the same as in section 4.1 The cantilever beam was meshed with 20 elements. Thus, the length of each element is *33.1 mm*. Moreover, each element was divided into *10* subdivisions, resulting in a Δx of *3.1mm* (see Appendix D, Figure D.1). A time step of *0.001 sec* was used for the simulation.

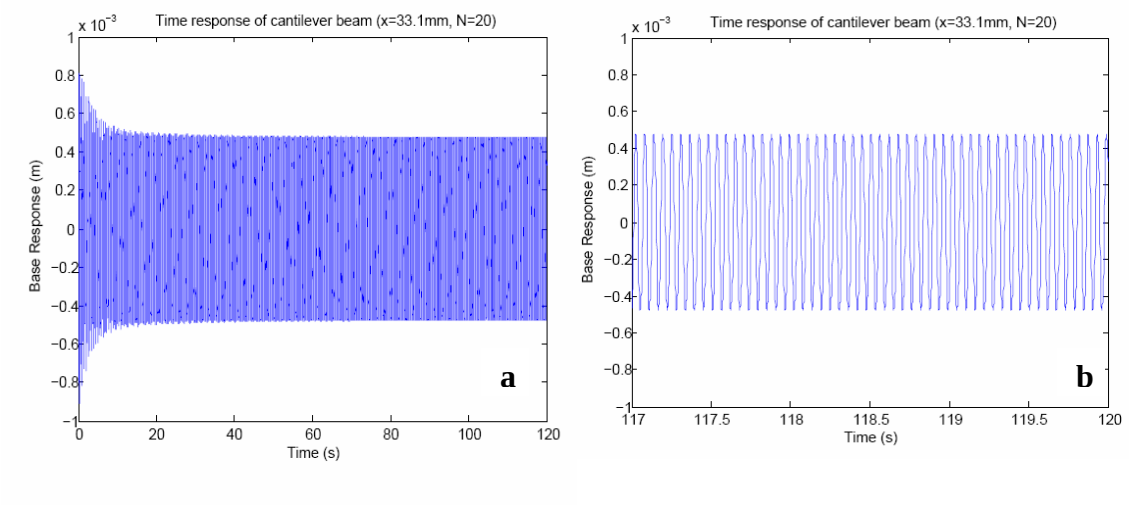

Figure 4. 4: Numerical time trace for x= 33.1 mm.

Figure 4.4 shows the time trace for a point *33.1 mm* from the base of the beam. For this simulation the excitation frequency and maximum acceleration at the base are *17.547 Hz* and *2.97g*, respectively. Most of the transient response dies out in the first *20* seconds of simulation. The transient response continues to decay at a slower rate from *t=20 sec* to *t= 80 sec* (Figure 4.4). For time greater than *80* seconds, the response is considered to be the steady state response.

Figure 4.4-b zooms into the last three seconds of the time response in Figure 4.4-a. The presence of a high frequency component is clear in Figure 4.4-b.

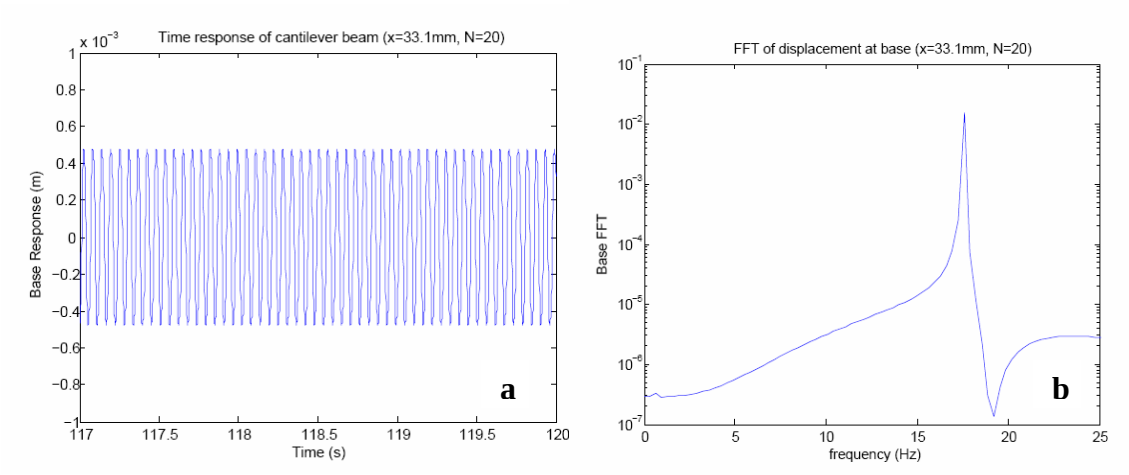

Figure 4. 5: Base response and FFT for Ω= 17.547 Hz, and a_b= 2.97g

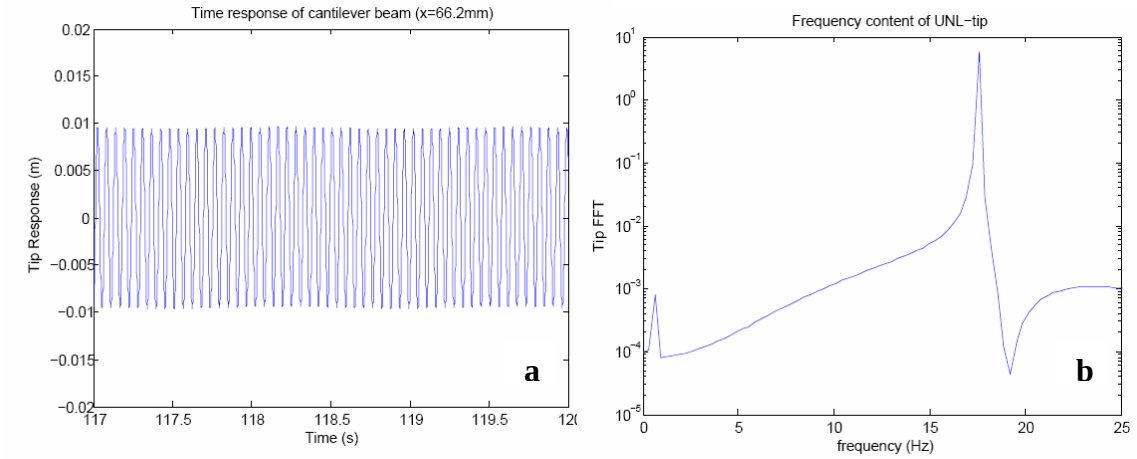

Figure 4. 6: Tip response and FFT for Ω= 17.547 Hz, and a_b= 2.97g

The FFT (Figure 4.5-b) for the last three seconds of simulation (Figure 4.5-a) shows two frequency components: one at *17.547 Hz* and another at *0.651 Hz*. Only the high frequency component is in agreement with the experimental results presented in section 4.1. However, there is no side band structure around the high frequency peak. Therefore, the high frequency component is not modulated.

Figure 4.6 shows the response and FFT for the tip of the beam. The high and low frequency components are centered at the same frequencies as the results at the base (Figure 4.5). However, the amplitude of the low frequency component at the tip of the beam (Figure 4.6-b) is significantly larger compared to the low frequency component at the base (Figure 4.5-b).

The FFT's for the numerical results were calculated using Matlab®. For this calculation, 512 points were sampled from the last three seconds of the time trace (Figures 4.5-a and 4.6-a). The number of sampled points is a power of 2, thus reducing the computation time for the FFT (Baher, 1990).

The numerical results show a high frequency component that is not modulated, and a low frequency component. These results do not agree with the experimental results obtained by Malatkar (2003). This discrepancy with the experimental results could be attributed to the presence of numerical error in the calculation of the nonlinear stiffness matrices kc_{ij} and ki_{ij} (3.14). Therefore, the numerical error in these matrices is investigated next.

The nonlinear stiffness matrices are defined in terms of the functions f_1 and f_2 given by

$$f_1 = (v'v'')', \quad f_2 = \frac{\partial^2}{\partial t^2}\int_l^s\int_0^s v'^2\, ds ds \tag{4.2}$$

In order to investigate the numerical error in the calculation of f_1 and f_2, these quantities are calculated for a displacement of the form

$$v(x,t) = A_1[\sinh\beta_1 x - \sin\beta_1 x - \varepsilon_1(\cosh\beta_1 x - \cos\beta_1 x)]\sin\Omega t \tag{4.3}$$

The bracketed term in (4.3) is simply the first linear mode shape for a cantilever beam (Appendix B). The constants A_1, β_1 and ε_1 are included in Table B.2. Substituting (4.3)

into (4.2) yields the analytical f_1 and f_2, which will be compared to the numerical f_1 and f_2, calculated as illustrated in Appendix D.

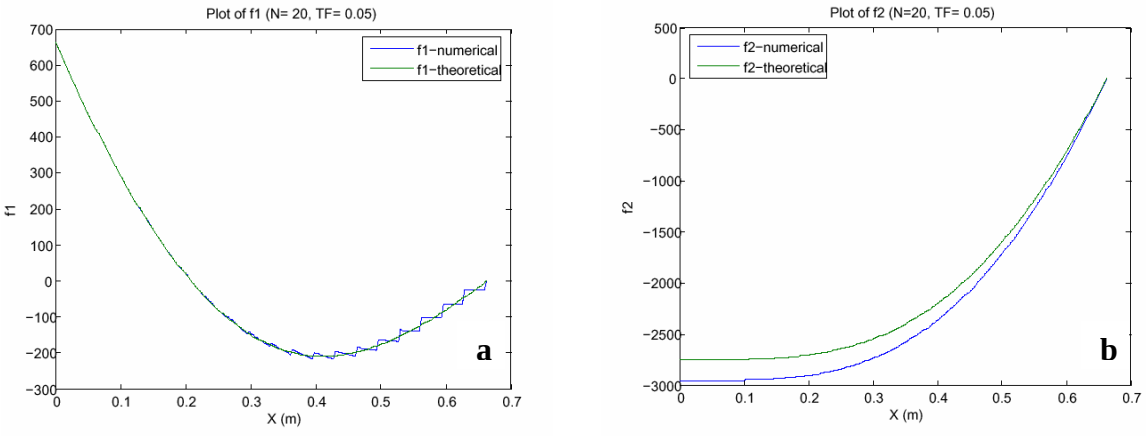

Figure 4. 7: Analytical and numerical f_1 and f_2

Figure 4.7 shows the analytical f_1 and f_2 compared against their numerical counterparts. The numerical f_1 and f_2 were calculated using 20 elements. There is numerical error in the calculation of f_1 (Figure 4.7-a). However, this numerical error is noticeable for $x > 300\ mm$. At $x = 33.1\ mm$, the point of interest for the time response, there is no significant error between the numerical and analytical f_1. Therefore, the numerical error in the calculation of f_1 does not affect the time response of the beam at the base.

There is a significant amount of numerical error in f_2 (Figure 4.7-b). This error is maximum at the base of the beam. Moreover the inertia nonlinearity, represented by f_2 , is known to dominate the response of the high frequency modes (Nayfeh and Pai, 2004). Hence, the significant amount of numerical error on this term contributes to the discrepancy between experimental and numerical results.

4.3 Transient Response

This section is devoted to the study of the transient response of the cantilever beam. The finite element model developed in ANSYS® is presented first. The results from this model are compared to results from the *NLB* program in Appendix A.

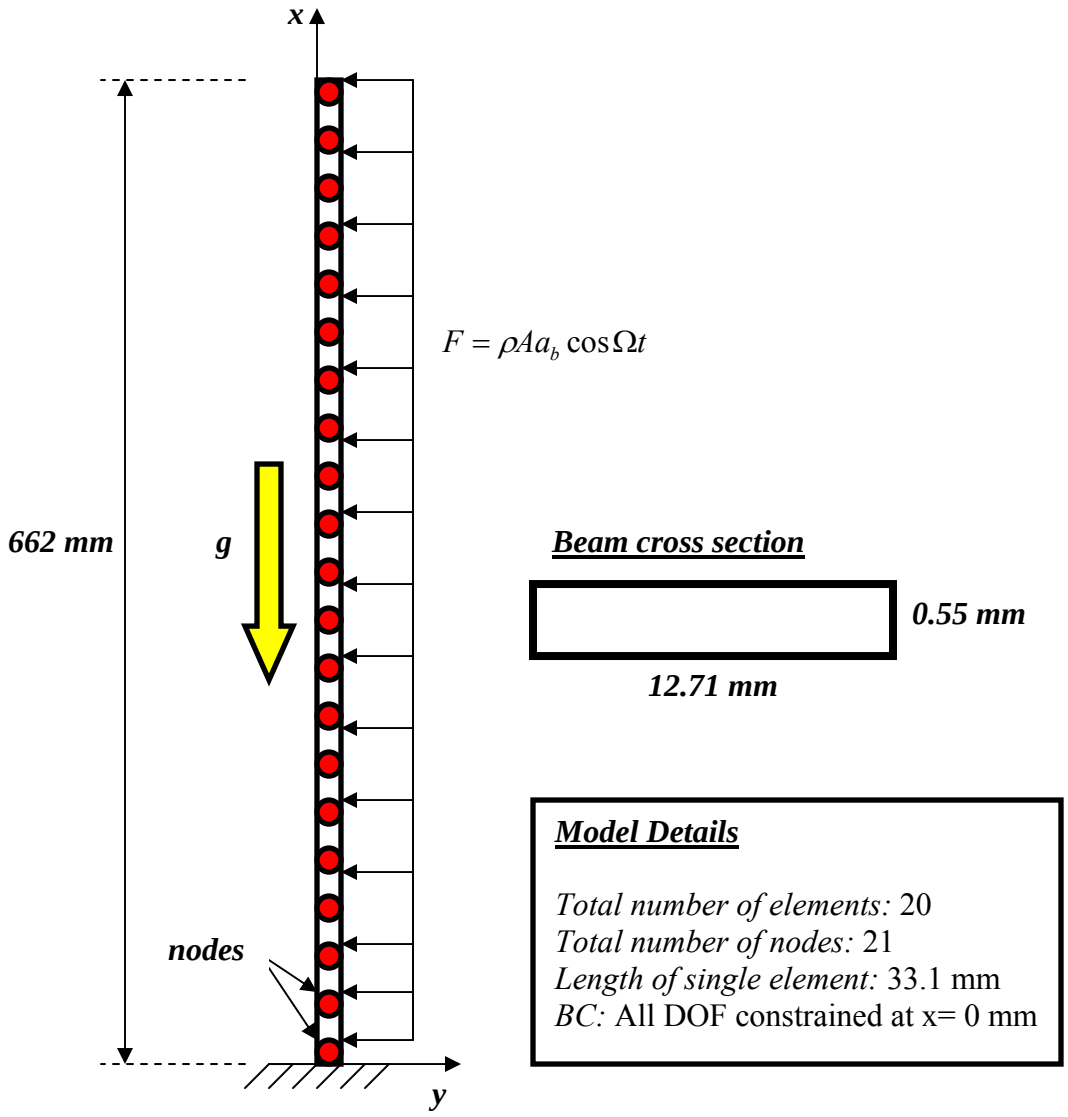

Figure 4. 8: Mesh and boundary conditions for ANSYS® model

Figure 4.8 shows the geometry used in the finite element model. The vertical beam has the same dimensions of the beam used by Malatkar (2003) to measure the experimental steady state response. Moreover, the beam is made of isotropic steel with properties as listed in section 4.1. The beam is meshed with *20* beam3[10] elements. Each element is *33.1 mm* long and has section properties calculated using the dimensions in Figure 4.8.

All degrees of freedom are constrained at the base of the beam (Figure 4.8). This is consistent with the boundary conditions of the problem (2.60). The effect of gravity is included in the simulation as shown in Figure 4.8.

The forcing function given by (4.1) is distributed evenly throughout all *21* nodes. The transient response of the beam is calculated for the first three seconds. The forcing function given in (4.1) is approximated as a series of straight lines. Figure 4.9 shows the approximation of one cycle of the forcing function. The cycle of the forcing function is divided into *14* load steps. This is a reasonable approximation of the exact function (Figure 4.9). A total of *739* load steps is required to obtain the transient response for the first three seconds.

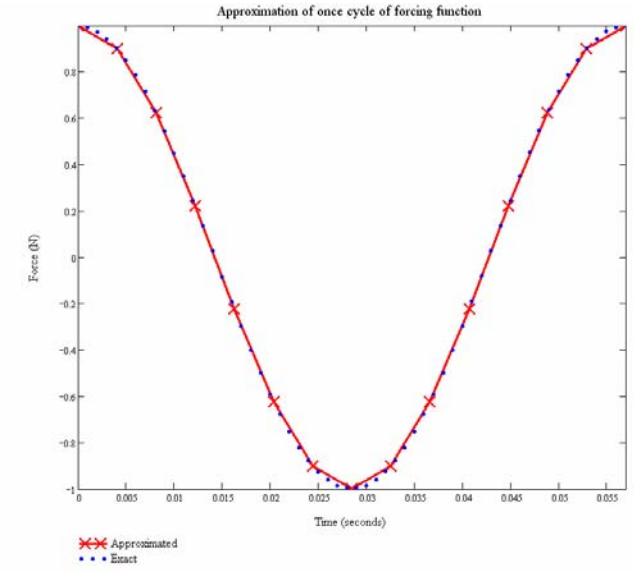

Figure 4. 9: Approximation of one cycle of the forcing function

[10] ANSYS® Theory Reference, Release 10.0 Documentation for ANSYS®

Figure 4.10 shows the response and FFT obtained in ANSYS®. The response plot (Figure 4.10-a) suggests the presence of multiple frequencies. The FFT[11] (Figure 4.10-b) reveals four frequencies dominating the time response.

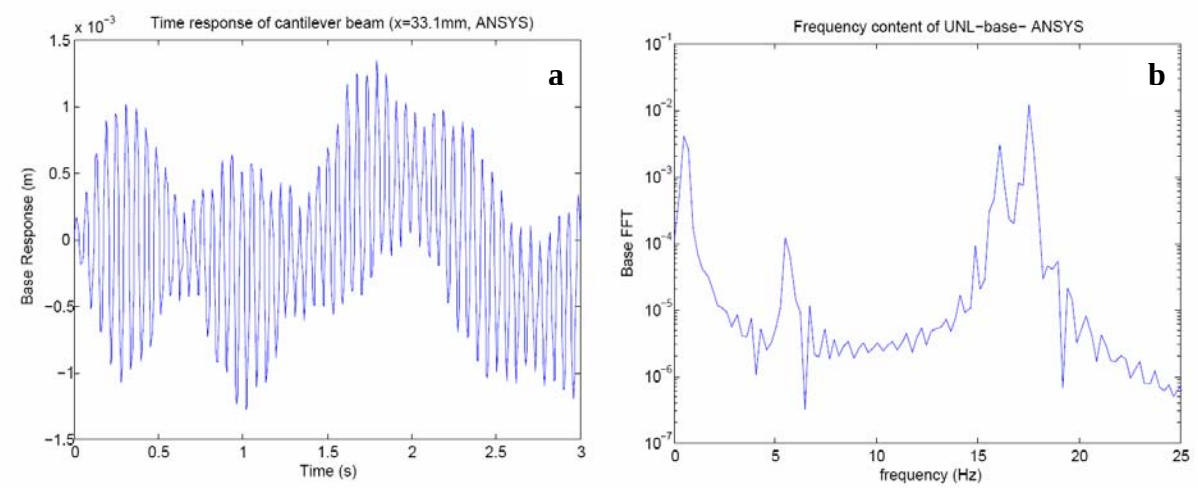

Figure 4. 10: Response and FFT from ANSYS®

The four peaks in the FFT (Figure 4.10-b) occur at *0.4798 Hz*, *5.518 Hz*, *16.07 Hz* and *17.51 Hz.*

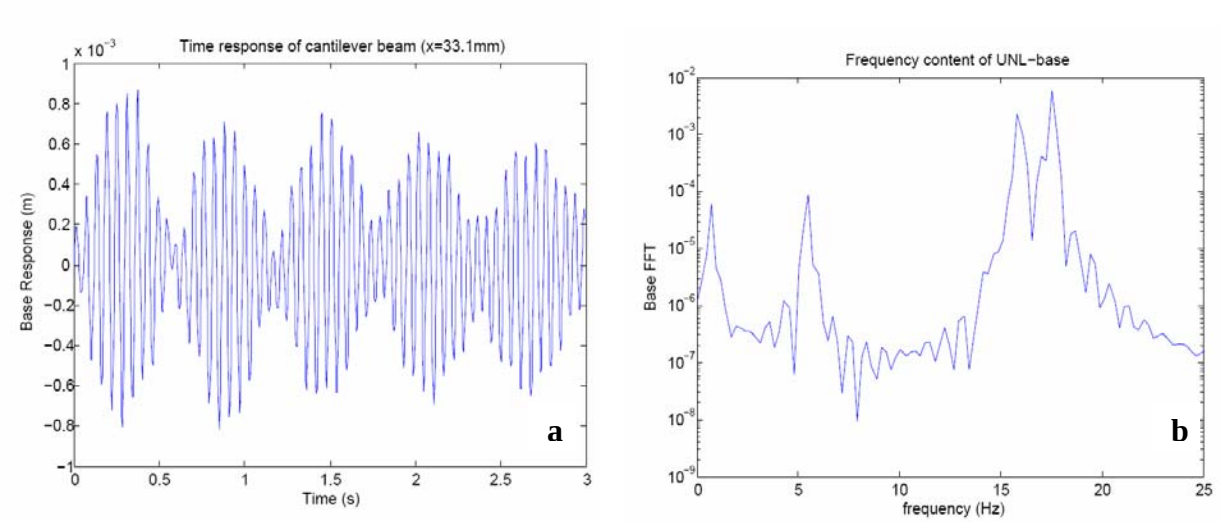

Figure 4. 11: Response and FFT from NLB

[11] FFT's were calculated in Matlab® using 512 points sampled from the transient response.

Figure 4.11 shows results obtained with *NLB*. The four frequencies that dominate the response are centered at *0.7197 Hz*, *5.518 Hz*, *15.83 Hz*, and *17.51 Hz*. A combined plot of the FFT obtained with ANSYS® (Figure 4.12) and the one obtained with *NLB* shows both FFT's are in agreement for the most part. The first frequency obtained with *NLB* is *50%* higher compared to ANSYS®. The remaining three frequencies are extremely close to the numerical results from *NLB*. Also, the first mode has a more significant participation in the time response obtained with ANSYS® (Figure 4.10), compared to the response obtained with *NLB* (Figure 4.11).

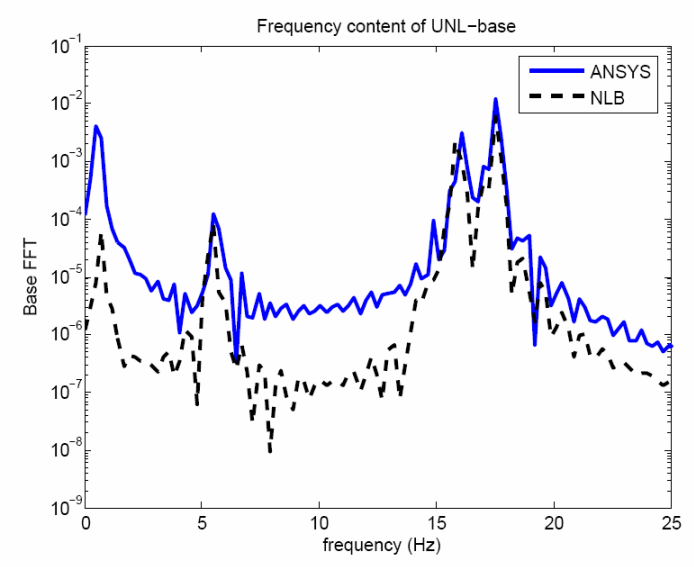

Figure 4. 12: Combined plot of FFT's

Chapter 5: Conclusion and Future Work

5.1 Conclusion

The time response of a vertically mounted, highly flexible, cantilever beam subjected to harmonic excitation at the base, was investigated. The equation of motion for the transverse nonlinear vibration of the beam, derived by Crespo da Silva and Glyn (1978), was solved numerically for the nonlinear displacement using a finite element model. This finite element model used Galerkin's weighted residuals method combined with the Newmark technique, and an iterative process, to obtain the nonlinear displacement of the beam.

The finite element model for the nonlinear transverse vibration of the beam was implemented in the program *NLB*[12]. This program was used to calculate the steady state response of the beam. The numerical results from the program were compared to the experimental results obtained by Malatkar (2003). The *NLB* program was also used to calculate the transient response of the beam, which was compared with the response obtained with ANSYS®.

The steady state response for the vertical cantilever beam was measured by Malatkar (2003) for an excitation frequency of *17.547 Hz*, which is close to the third natural frequency of the beam. The FFT of the experimental results shows a modulated high frequency component centered at *17.547 Hz*, and a low frequency component centered at *1.58 Hz*. Moreover, the modulation frequency for the high frequency component is equal to the low frequency component, i.e., *1.58 Hz*.

The FFT for the steady state response computed with the program *NLB* shows a high frequency component centered at *17.547 Hz*. Unlike the experimental results from Malatkar (2003), this high frequency component is not modulated. The absence of

[12]Non Linear Beam

modulation in the high frequency component is attributed to the presence of numerical error in the computation of the nonlinear inertia term. Nayfeh and Pai (2004) showed that the nonlinear inertia term dominates the response of the third mode in a highly flexible beam. The FFT for the numerical results also shows a low frequency component centered at *0.651 Hz*. This result is not in agreement with the experimental results.

The transient response for the first three seconds, obtained with ANSYS® , is dominated by four frequency components centered at *0.4798 Hz, 5.518 Hz, 16.07 Hz,* and *17.51 Hz.* The transient response determined with *NLB* is dominated by frequency components centered at *0.7197 Hz, 5.518 Hz, 15.83 Hz,* and *17.51 Hz.* These results are in agreement with ANSYS® except for the first frequency component, which is *50%* higher with *NLB*.

In summary, the numerical results obtained with *NLB* differ from the experimental results (Malatkar, 2003) due to the presence of numerical error in the former. The transient response calculated with *NLB* agrees with the response calculated with ANSYS® for the most part.

5.2 Future Work

The program *NLB* needs to be streamlined to reduce computation time of the steady state response. Also, the numerical error in the calculation of the nonlinear inertia term should be improved by using alternate numerical methods for its calculation.

Bibliography

1 Anderson, T.J., et al., *Nonlinear Resonances in a Flexible Cantilever Beam*, Nonlinear Vibrations, ASME, Vol. 50, pp. 109-116, 1992

2 Anderson, T.J., et al., *Observations of Nonlinear Interactions in a Flexible Cantilever Beam,* Proceedings of the 33rd AIAA Structures, Structural Dynamics & Materials Conference, AIAA paper no. 92-2332-CP, Dallas, Tx, pp. 1678-1686

3 *ANSYS® Theory Reference*, Release 10.0 Documentation for ANSYS®

4 Baher, H., *Analog and Digital Signal Processing*, John Wiley & Sons, New York, 1990

5 Bathe, K.J., and Wilson, E.L., *Stability and Accuracy Analysis of Direct Integration Methods,* Earthquake Engineering and Structural Dynamics, Vol. 1, pp. 283-291, 1973

6 Blevins, R.D., *Formulas for Natural Frequency and Mode Shape*, Van Nostrand Reinhold Company, New York, 1979

7 Borse, G.J., *Numerical Methods with Matlab*, PWS-Kent, Boston, 1997

8 Budynas, R.G., *Advanced Strength and Applied Stress Analysis*, McGraw-Hill, New York, 1999

9 Cook, R.D., and Young, W.C., *Advanced Mechanics of Materials*, Prentice Hall, New Jersey, 1999

10 Cook, R.D., *Finite Element Analysis for Stress Analysis*, John Wiley & Sons, New York, 1995

11 Crespo da Silva, M.R.M., and Glynn, C.C., *Nonlinear Flexural-Flexural-Torsional Dynamics of Inextensional Beams. I. Equations of Motion,* Journal of Structural Mechanics, Vol. 6, pp. 437-448, 1978

12 Crespo da Silva, M.R.M., and Glynn, C.C., *Nonlinear Non-Planar Resonant Oscillations in Fixed-Free Beams with Support Asymmetry,* International Journal of Solids Structures, Vol. 15, pp. 209-219, 1979

13 Crespo da Silva, M.R.M., and Glynn, C.C., *Out-of Plane Vibrations of a Beam Including Nonlinear Inertia and Non-Linear Curvature Effects,* International Journal of Non-Linear Mechanics, Vol. 13, pp. 261-271, 1979

14 Crespo da Silva, M.R.M., and Glynn. C.C., *Nonlinear Flexural-Flexural-Torsional Dynamics of Inextensional Beams. II. Forced Motions,* Journal of Structural Mechanics, Vol. 6, pp. 449-461, 1978

15 Kim, M.G., et al. *Non-planar Nonlinear Vibration Phenomenon on the One to One Internal Resonance of the Circular Cantilever Beam,* Key Engineering Materials, Vols. 326-328, pp. 1641-1644, 2006

16 Kreyzig, E., *Advanced Engineering Mathematics*, John Wiley & Sons, Massachusetts, 1999

17 Love, A.E.H., *A Treatise on the Mathematical Theory of Elasticity,* Dover Publications, New York, 1944

18 Malatkar, P., and Nayfeh, A.H., *On the Transfer of Energy Between Widely Spaced Modes in Structures,* Nonlinear Dynamics, Vol. 31, pp. 225-242, 2003

19 Malatkar, P., *Nonlinear Vibrations of Cantilever Beams and Plates,* Ph.D. thesis, Virginia Polytechnic Institute and State University, 2003

20 Mase, G.E., *Continuum Mechanics*, McGraw-Hill, New York, 1970

21 Meirovitch, L., *Fundamentals of Vibrations*, McGraw-Hill, New York, 2001
22 Nayfeh, A.H., and Arafat, H.N., *Nonlinear response of cantilever beams to combination and subcombination resonances,* Shock and Vibration, Vol. 5, pp. 277-288, 1998
23 Nayfeh, A.H., and Pai, P.F., *Linear and Nonlinear Structural Mechanics,* John Wiley & Sons, New York, 2003
24 Nayfeh, S.A., and Nayfeh, A.H., *Nonlinear Interactions Between Two Widely Spaced Modes- External Excitation,* International Journal of Bifurcation and Chaos, Vol. 3, No.2, pp. 417-427, 1993
25 Rao, S.S., *Mechanical Vibrations*, Addison Wesley, New York, 1990
26 Reddy, J.N., *An Introduction to the Finite Element Method*, McGraw-Hill, New York, 1993
27 Thomson, W.T., and Dahleh, M.D., *Theory of Vibration with Applications*, Prentice Hall, New Jersey, 1998
28 Török, J.S., *Analytical Mechanics*, John Wiley & Sons, New York, 2000
29 Zienkiewicz, O.C., *A New Look at the Newmark, Houbolt and Other Time Stepping Formulas. A Weighted Residual Approach,* Earthquake Engineering and Structural Dynamics, Vol. 5., pp. 413-418, 1977
30 Zienkiewicz, O.C., *The Finite Element Method*, McGraw-Hill, London, 1977
31 Zill, D.G., et al., *Differential Equations with Boundary Value Problems,* Brooks/Cole Publishing Company, New York, 1997

Appendix A: NLB Matlab® Program

```
%Nonlinear Vibration of a Cantilever Beam
%Written by Ivan Delgado-Velazquez
L= 0.662; W= 0.01271; tk= 5.5e-4; %beam dimensions
rho= 7400; E= 165.5e9; %material properties
Alpha1= 0.064; Alpha2= 4.72e-5; %proportional damping coefficients
N= 20; h= L/N; numX=10; deltax= h/numX; %elements variables
TOL=0.01; %convergence criterion for nonlinear loop
deltat= 0.001;  tf=3; k= tf/deltat; %time variables
g=9.81; ab= 2.97*g; OMEGA= 17.547; %force variables
Area= W*tk;  I= 1/12*W*tk^3; %section properties
%shape functions and derivatives
xs=0:deltax:h;
PSI(:,1)= 1 - (3/h^2)*xs.^2 + (2/h^3)*xs.^3;
PSI(:,2)= h*((xs/h) -(2/h^2)*xs.^2 + (1/h^3)*xs.^3);
PSI(:,3)= (3/h^2)*xs.^2 - (2/h^3)*xs.^3;
PSI(:,4)= h*(-(1/h^2)*xs.^2 + (1/h^3)*xs.^3);
PSIP(:,1)= -6*(xs/h^2) + (6/h^3)*xs.^2;
PSIP(:,2)= 1 - 4*(xs/h) + (3/h^2)*xs.^2;
PSIP(:,3)= 6*(xs/h^2) - (6/h^3)*xs.^2;
PSIP(:,4)= - 2*(xs/h) + (3/h^2)*xs.^2;
xs4=0:deltax/4:h;
PSIP_f2_4(:,1)= -6*(xs4/h^2) + (6/h^3)*xs4.^2; %FOR EVALUATION OF f2 ONLY
PSIP_f2_4(:,2)= 1 - 4*(xs4/h) + (3/h^2)*xs4.^2;
PSIP_f2_4(:,3)= 6*(xs4/h^2) - (6/h^3)*xs4.^2;
PSIP_f2_4(:,4)= - 2*(xs4/h) + (3/h^2)*xs4.^2;
PSIPP(:,1)= -6/h^2 + (12/h^3)*xs;
PSIPP(:,2)= -4/h + (6/h^2)*xs;
PSIPP(:,3)= 6/h^2 - (12/h^3)*xs;
PSIPP(:,4)= -2/h + (6/h^2)*xs;
PSIPPP(:,1)= (12/h^3)*ones(1,(h/deltax)+1);
PSIPPP(:,2)= (6/h^2)*ones(1,(h/deltax)+1);
PSIPPP(:,3)= -(12/h^3)*ones(1,(h/deltax)+1);
PSIPPP(:,4)= (6/h^2)*ones(1,(h/deltax)+1);
Me= (rho*Area*h/420)*[156 22*h 54 -13*h; 22*h 4*h*h 13*h -3*h*h;
                      54 13*h 156 -22*h; -13*h -3*h*h -22*h 4*h*h];
Ke= (E*I/h^3)*[12 6*h -12 6*h; 6*h 4*h*h -6*h 2*h*h;
               -12 -6*h 12 -6*h; 6*h 2*h*h -6*h 4*h*h];
Ce= Alpha1*Me + Alpha2*Ke; %element matrices - [M], [KL], [C]
Gamma= 0.5; Beta= 0.25; %Newmark coefficients
epsilon= 0.5-2*Beta + Gamma;     PHI= rho*Area*ab;
delta= 0.5 + Beta - Gamma;       THETA= 2*pi*OMEGA;
%global matrices - [M], [KL], [C]
z= 2*(N+1);
```

```
Mg= zeros(z); Kg= zeros(z); Cg= zeros(z);
x1= 1;
for x=1:N
   a=1;
   for i=x1:x1+3
      b=1;
      for j=x1:x1+3
         Mg(i,j)=Mg(i,j)+ Me(a,b);
         Kg(i,j)=Kg(i,j)+ Ke(a,b);
         Cg(i,j)=Cg(i,j)+ Ce(a,b);
         b= b+1;
      end
      a= a+1;
   end
   x1= x1 +2;
end
%reduced global matrices
for i=1:z-2
   for j=1:z-2
      MgR(i,j)= Mg(i+2,j+2);
      KgR(i,j)= Kg(i+2,j+2);
      CgR(i,j)= Cg(i+2,j+2);
   end
end
%Newmark matrices - LINEAR
A1= MgR + Gamma*deltat*CgR + Beta*deltat^2*KgR;
A2= -2*MgR + (1-2*Gamma)*deltat*CgR + epsilon*deltat^2*KgR;
A3= MgR - (1-Gamma)*deltat*CgR + delta*deltat^2*KgR;
%Force discretization vector
FF= zeros(z,1);
a=0;
for ll=1:N
   for aa=1:4
      S1=0; S2=0;
      for l=1:(h/deltax +1)
         alpha(l)= PSI(l,aa);
      end
      for i1=2:2:h/deltax
         S1= S1 + alpha(i1);
      end
      for j1=3:2:h/deltax -1
         S2= S2 + alpha(j1);
      end
      SS(aa)=(deltax/3)*(alpha(1)+ 4*S1+2*S2+ alpha(h/deltax+1));
   end
   for i1=1:4
```

```
        FF(i1+a)= FF(i1+a) + SS(i1);
    end
    a= a+2;
    for i1=1:z-2
        FD(i1,1)= FF(i1+2);
    end
end
UL(:,1)= zeros(z,1);   %from IC
time= 0:deltat:tf; %time vector
%Main loop
for j=1:k
    %Linear loop
    for o=1:z-2
        for p=1:j
            ULr(o,p)= UL(o+2,p);
        end
    end
    if j==1
        U0= ULr(:,1); U1= ULr(:,1);
        F0= zeros(z-2,1);
        FLin(:,j)= PHI*FD*cos(THETA*time(j));
        F1= FLin(:,j);
    else
        U0= ULr(:,j-1);  U1= ULr(:,j);
        F0= FLin(:,j-1);  F1= FLin(:,j);
    end
    FLin(:,j+1)= PHI*FD*cos(THETA*time(j+1));
    F2= FLin(:,j+1);
    F= Beta*F2 + epsilon*F1 + delta*F0;
    U2= -inv(A1)*A2*U1 - inv(A1)*A3*U0 + deltat^2*inv(A1)*F;
    ULr(:,j+1)= U2;
    for i=1:z
        for p=1:j+1
            if i<= 2
                UL(i,p)=0;
            else
                UL(i,p)= ULr(i-2,p);
            end
        end
    end
    %Nonlinear loop
    eps= 10^5; counter= 0;
    while eps > TOL
        %first nonlinear stiffness matrix
        a1= 1; b0= 0;
        for o=1:N
```

```
    for p= 1:(h/deltax)+1
        WWP(p)= PSIP(p,1)*UL(a1,j+1) + PSIP(p,2)*UL(a1+1,j+1)+...
            PSIP(p,3)*UL(a1+2,j+1) + PSIP(p,4)*UL(a1+3,j+1);
        WWPP(p)= PSIPP(p,1)*UL(a1,j+1)+ PSIPP(p,2)*UL(a1+1,j+1)+...
            PSIPP(p,3)*UL(a1+2,j+1) + PSIPP(p,4)*UL(a1+3,j+1);
        WWPPP(p)= PSIPPP(p,1)*UL(a1,j+1)+ PSIPPP(p,2)*...
            UL(a1+1,j+1)+PSIPPP(p,3)*UL(a1+2,j+1) + ...
            PSIPPP(p,4)*UL(a1+3,j+1);
        WP(p+b0)= WWP(p);
        WPP(p+b0)= WWPP(p);
        WPPP(p+b0)= WWPPP(p);
    end
    a1= a1+2;
    b0= b0 + h/deltax;
end
AA= N*(h/deltax + 1)- N +1;
AA_f2_2= N*(2*h/deltax + 1)- N +1;
AA_f2_4= N*(4*h/deltax + 1)- N +1;
f1= WP.*WPPP + WPP.^2;
f1(AA)= 0; %from BC
aaa=0; bbb=0; mmm=0; KNL1=zeros(z);
for o=1:N
    for pp=1:4
        for qq=1:4
            S1=0; S2=0;
            for l=1:(h/deltax)+1
                PsiPijF1(l)= PSIP(l,pp)*PSIP(l,qq)*f1(mmm+l);
            end
            for ii=2:2:(h/deltax)
                S1= S1 + PsiPijF1(ii);
            end
            for ii=3:2:(h/deltax - 1)
                S2= S2 + PsiPijF1(ii);
            end
            KKNL(pp,qq)= (deltax/3)*(PsiPijF1(1)+ 4*S1+2*S2 + ...
                PsiPijF1(h/deltax+1));
            KNL1(pp+aaa,qq+bbb)= KNL1(pp+aaa,qq+bbb)+ KKNL(pp,qq);
        end
    end
    aaa= aaa+2; bbb= bbb+2; mmm= mmm + h/deltax;
end
KNL1= E*I*KNL1; %first nonlinear stiffness matrix
for ii=1:z-2
    for jj=1:z-2
      KNL1r(ii,jj)= KNL1(ii+2,jj+2); %reduced KNL1
    end
```

```
end
%second nonlinear stiffness matrix
if j == 1
   WPsq2Dot= Wpsq2Dot_approx_SS; %approx. with lin. disp.
else
   a1= 1; b0= 0;
   for o=1:N
      for p= 1:(4*h/deltax)+1
         wWP(p,3)= PSIP_f2_4(p,1)*UL(a1,j+1)+PSIP_f2_4(p,2)*...
            UL(a1+1,j+1)+PSIP_f2_4(p,3)*UL(a1+2,j+1) +...
            PSIP_f2_4(p,4)*UL(a1+3,j+1);
         wWP(p,2)= PSIP_f2_4(p,1)*UL(a1,j) + PSIP_f2_4(p,2)*...
            UL(a1+1,j)+PSIP_f2_4(p,3)*UL(a1+2,j) +...
            PSIP_f2_4(p,4)*UL(a1+3,j);
         wWP(p,1)= PSIP_f2_4(p,1)*UL(a1,j-1)+PSIP_f2_4(p,2)*...
            UL(a1+1,j-1)+PSIP_f2_4(p,3)*UL(a1+2,j-1) +...
            PSIP_f2_4(p,4)*UL(a1+3,j-1);
         wP(p+b0,3)= wWP(p,3); wP(p+b0,2)= wWP(p,2);
         wP(p+b0,1)= wWP(p,1);
      end
      a1= a1+2;
      b0= b0 + 4*h/deltax;
   end
   for ii=1:AA_f2_4
      for jj=1:3
         WPsq(ii,jj)= wP(ii,jj)*wP(ii,jj);
      end
   end
   for ii=1:AA_f2_4
      WPsqDot(ii,1)= (WPsq(ii,2)-WPsq(ii,1))/deltat;
      WPsqDot(ii,2)= (WPsq(ii,3)-WPsq(ii,2))/deltat;
      WPsq2Dot(ii)= (WPsqDot(ii,2)-WPsqDot(ii,1))/deltat;
   end
end
xx1=1;
for xx=1:2:AA_f2_4
   S1=0; S2=0; i1=2; j1=3;
   while i1<= xx-1
      S1= S1 + WPsq2Dot(i1);
      i1= i1 + 2;
   end
   while j1<= xx-2
      S2= S2 + WPsq2Dot(j1);
      j1= j1 + 2;
   end
   SS1(xx1)=(deltax/12)*(WPsq2Dot(1)+4*S1 + 2*S2 + WPsq2Dot(xx));
```

```
   xx1=xx1+1;
end
SS1(1)=0;
xx2=1;
for xx=1:2:AA_f2_2
   S1=0; S2=0; i1=xx+1; j1=xx+2;
   while i1<= AA_f2_2 - 1
      S1= S1 + SS1(i1);
      i1= i1 + 2;
   end
   while j1<= AA_f2_2 - 2
      S2= S2 + SS1(j1);
      j1= j1 + 2;
   end
   f2(xx2)=(-deltax/6)*(SS1(xx) + 4*S1 + 2*S2 + SS1(AA_f2_2));
   xx2=xx2+1;
end
f2(AA)= 0;
aaa=0; bbb=0; mmm=0; KNL2=zeros(z);
for o=1:N
   for pp=1:4
      for qq=1:4
         S1=0; S2=0;
         for l=1:(h/deltax)+1
            PsiPijF2(l)= PSIP(l,pp)*PSIP(l,qq)*f2(mmm+l);
         end
         for ii=2:2:(h/deltax)
            S1= S1 + PsiPijF2(ii);
         end
         for ii=3:2:(h/deltax - 1)
            S2= S2 + PsiPijF2(ii);
         end
         KKnl(pp,qq)= (deltax/3)*(PsiPijF2(1)+ 4*S1+2*S2 + ...
            PsiPijF2(h/deltax+1));
         KNL2(pp+aaa,qq+bbb)= KNL2(pp+aaa,qq+bbb)+ KKnl(pp,qq);
      end
   end
   aaa= aaa+2; bbb= bbb+2; mmm= mmm + h/deltax;
end
KNL2= 0.5*rho*Area*KNL2; %second nonlinear stiffness matrix
for ii=1:z-2
   for jj=1:z-2
     KNL2r(ii,jj)= KNL2(ii+2,jj+2); %reduced KNL2
   end
end
KTotal= KgR-KNL1r-KNL2r; %total stiffness matrix
```

```
CNL= Alpha1*MgR + Alpha2*KTotal; %nonlinear damping matrix
%nonlinear displacement - Newmark technique
for o=1:z-2
   for p=1:j
      UNLr(o,p)= UL(o+2,p);
   end
end
if j==1
   U0= UNLr(:,1); U1= UNLr(:,1);
   F0= zeros(z-2,1);
   FNLin(:,j)= FLin(:,j);
   F1= FNLin(:,j);
else
   U0= UNLr(:,j-1);  U1= UNLr(:,j);
   F0= FNLin(:,j-1);  F1= FNLin(:,j);
end
%Newmark matrices - NONLINEAR
A1NL= MgR + Gamma*deltat*CNL + Beta*deltat^2*KTotal;
A2NL= -2*MgR + (1-2*Gamma)*deltat*CNL + epsilon*deltat^2*KTotal;
A3NL= MgR - (1-Gamma)*deltat*CNL + delta*deltat^2*KTotal;
%total force vector
X= 0:deltax:L; %global X vector
for ii=1:AA
   f3(ii)= (X(ii)*deltax - L)*WPP(ii) + WP(ii);
end
G= zeros(z,1);
a=0; m=0;
for ll=1:N
   for aa=1:4
      S1=0; S2=0;
      for l=1:(h/deltax +1)
         alpha(l)= PSI(l,aa)*f3(m+l);
      end
      for i1=2:2:h/deltax
         S1= S1 + alpha(i1);
      end
      for j1=3:2:h/deltax -1
         S2= S2 + alpha(j1);
      end
      SS(aa)=(deltax/3)*(alpha(1)+ 4*S1+2*S2 + ...
         alpha(h/deltax+1));
   end
   for i1=1:4
      G(i1+a)= G(i1+a) + SS(i1);
   end
   a= a+2; m= m+h/deltax;
```

```
        end
        G= rho*Area*g*G; %gravity vector
        for i1=1:z-2
            Gr(i1)= G(i1+2);
        end
        FNLin(:,j+1)= FLin(:,j+1)+ Gr'; %nonlinear force vector
        F2= FNLin(:,j+1);
        F= Beta*F2 + epsilon*F1 + delta*F0;
        U2= -inv(A1NL)*A2NL*U1 - inv(A1NL)*A3NL*U0 + deltat^2*inv(A1NL)*F;
        UNLr(:,j+1)= U2;
        for i=1:z
            for p=1:j+1
                if i<= 2
                    UNL(i,p)=0;
                else
                    UNL(i,p)= UNLr(i-2,p);
                end
            end
        end
        for ii=1:z
            DELTA(ii)= abs(UL(ii,j+1) - UNL(ii,j+1));
        end
        eps= sum(DELTA);
        UL(:,j+1)= UNL(:,j+1);
        counter=counter +1;
    end
    kounter(j)=counter; %number of iterations in NL loop
    EPS(j)= eps; %convergence variable for each time step
    time(j)
end
%time response plots
Response_base= UL(3,:); %response of base (2nd node)
Response_tip= UL(z-1,:); %response of tip (last node)
figure
plot(time,Response_base)
xlabel('Time (s)'), ylabel('Base Response (m)')
title('Time response of cantilever beam (x=33.1mm)') %figure 1
figure
plot(time,Response_tip)
xlabel('Time (s)'), ylabel('Tip Response (m)')
title('Time response of cantilever beam (x=66.2mm)') %figure 2
%Fast Fourier Transform (FFT)
Trecord= 3; %length of time record
TI= tf- Trecord; %initial time of sampling
TF= tf; %final time of sampling
Ta= TI/deltat +1; %element number corresponding to TI
```

```
Tb= TF/deltat +1; %element number corresponding to TF
SR= 6; %sampling rate
DELTAT= SR*deltat; %sampling interval
fs= 1/(DELTAT); %sampling frequency
ii=1;
for i=Ta:SR:Tb
   Response_baseS(ii)= Response_base(i); %sampled points for FFT
   Response_tipS(ii)= Response_tip(i); %sampled points for FFT
   ii=ii+1;
end
Yb= fft(Response_baseS,512);
FB= Yb.*conj(Yb);
Yt= fft(Response_tipS,512);
FT= Yt.*conj(Yt);
figure
freq = fs*(0:256)/512;
plot(freq,FT(1:257))
xlabel('frequency (Hz)'), ylabel('Tip FFT')
title('Frequency content of UNL-tip') %figure 3
figure
freq = fs*(0:256)/512;
plot(freq,FB(1:257))
xlabel('frequency (Hz)'), ylabel('Base FFT')
title('Frequency content of UNL-base') %figure 4
```

Appendix B: Linear Natural Frequencies and Mode Shapes

The first four linear mode shapes and natural frequencies for the cantilever beam in Figure B.1 are calculated next. Both the mode shapes and natural frequencies are required to calculate the linear forced analytical response of the beam, which is the topic of Appendix C.

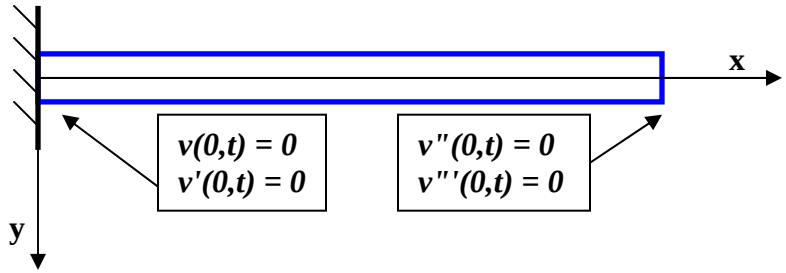

Figure B. 1: Cantilever beam and boundary conditions

The linear equation of motion for the free flexural vibration of the cantilever beam is given by

$$(EIv'')''+\rho A\ddot{v} = 0 \tag{B.1}$$

where *E, I, A* and ρ are the Young's modulus, area moment of inertia, cross sectional area and density, respectively. For uniform properties the equation can be written as

$$v^{iv} + \frac{\rho A}{EI}\ddot{v} = 0 \tag{B.2}$$

Assuming the transverse displacement *v* is of the form given by

$$v = V(x)e^{i\omega t} \tag{B.3}$$

where ω is the frequency of vibration, and substituting (B.3) into (B.2) results in

$$V^{iv} - \beta^4 V = 0 \tag{B.4}$$

where β is related to *E, I, A*,ρ, and ω through

$$\beta^4 = \frac{\rho A}{EI}\omega^2 \tag{B.5}$$

Equation (B.4) is a linear ordinary differential equation with constant coefficients. Thus, the characteristic equation of (B.4) is (Kreyszig, 1999)

$$V(x) = A\sinh\beta x + B\cosh\beta x + C\sin\beta x + D\cos\beta x \tag{B.6}$$

where *A, B, C,* and *D* are constants. The first three derivatives of (B.6) are

$$\begin{aligned} V'(x) &= A\beta\cosh\beta x + B\beta\sinh\beta x + C\beta\cos\beta x - D\beta\sin\beta x \\ V''(x) &= A\beta^2\sinh\beta x + B\beta^2\cosh\beta x - C\beta^2\sin\beta x - D\beta^2\cos\beta x \\ V'''(x) &= A\beta^3\cosh\beta x + B\beta^3\sinh\beta x - C\beta^3\cos\beta x + D\beta^3\sin\beta x \end{aligned} \tag{B.7}$$

Substituting the boundary conditions listed in Figure B.1 into equations (B.6) and (B.7) yields

$$B = -D \ , \quad A = -C \tag{B.8}$$

$$B = \frac{-(\sinh\theta + \sin\theta)}{(\cosh\theta + \cos\theta)}A \tag{B.9}$$

Further manipulation of equations (B.6) through (B.9) yields

$$\cos\theta = -\cosh^{-1}\theta \tag{B.10}$$

where θ is the product βl. Moreover, substituting (B.8) into (B.6) results in

$$V(x) = A(\sinh(\beta x) - \sin(\beta x)) + B(\cosh(\beta x) - \cos(\beta x)) \qquad \text{(B.11)}$$

Equation (B.10) is solved graphically for the natural frequencies of the beam. This is done by plotting both sides of the equation against the variable θ. Figure (B.2) shows a plot of both sides of equation (B.10). The natural frequencies are calculated from the values of θ where both curves intersect.

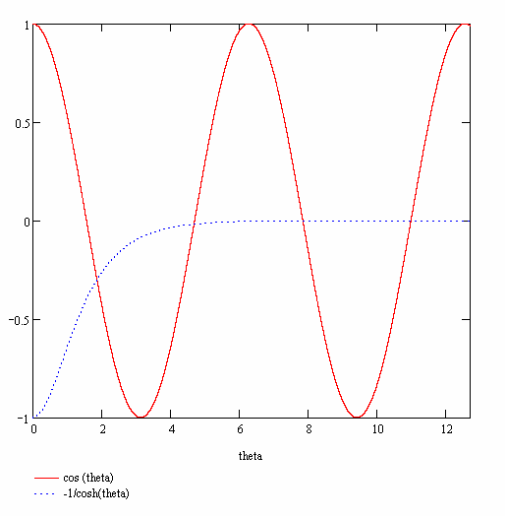

Figure B. 2: Plot used to obtain natural frequencies

Table B. 1: Natural frequencies of linear cantilever beam			
Mode number	*θ (rad)*	*f_n- graphical (Hz)*	*f_n - exact (Hz)*
1	1.88	0.96	0.959
2	4.7	6.02	6.008
3	7.85	16.8	16.824
4	11	33	32.961

The natural frequencies obtained from equation (B.10) are presented in Table B.1. These natural frequencies are compared against the exact values provided by Rao (1990). The frequencies obtained from (B.10) are extremely close to the exact frequencies.

The mode shapes of the cantilever beam are obtained by substituting (B.9) into (B.11), along with the appropriate θ from Table B.1. Thus, the r^{th} mode shape is given by

$$^{*}V_r(x) = A_r[\sinh\beta_r x - \sin\beta_r x - \varepsilon_r(\cosh\beta_r x - \cos\beta_r x)] \tag{B.12}$$

with ε_r given by

$$\varepsilon_r = \frac{-(\sinh\theta_r + \sin\theta_r)}{(\cosh\theta_r + \cos\theta_r)} \tag{B.13}$$

The asterisk in $^{*}V_r(x)$ indicates the mode shape is normalized.

The constants A_r in (B-12) are obtained using the orthogonality relation given by (Meirovitch, 2001)

$$\int_0^l {}^{*}V_r\, \rho A\, {}^{*}V_r\, dx = 1 \tag{B.14}$$

where ρ and A are the density and cross sectional area, respectively. Substituting (B.12) into (B.14) and solving for A_r yields

$$A_r = \sqrt{\frac{1}{\rho A I_r}} \tag{B.15}$$

where the quantity I_r is simply the integral

$$I_r = \int_0^l (\sinh(\beta_r x) - \sin(\beta_r x) - \varepsilon_r \cosh(\beta_r x) + \varepsilon_r \cos(\beta_r x))^2\, dx \tag{B.16}$$

The values of A_r, β_r, and ε_r for the first four modes are included in Table B.2. These values are used in Appendix C to write the forced response of the beam in terms of the first four mode shapes.

Table B. 2: Constants for the first four mode shapes

r	A_r	β_r	ε_r
1	3.967	2.84	1.36
2	5.504	7.1	0.982
3	5.4	11.86	1
4	5.404	16.62	1

Appendix C: Forced Vibration of a Cantilever Beam

The forced response of a cantilever beam subjected to harmonic excitation at the base (Figure C.1) is presented next. The cantilever beam is made of isotropic material and has uniform properties.

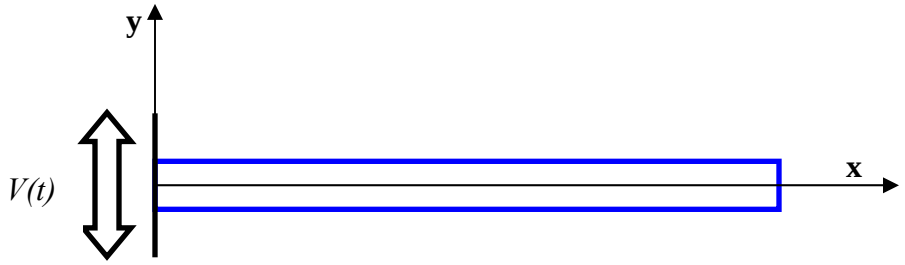

Figure C. 1: Cantilever beam subjected to base excitation

From Appendix B, the linear equation of motion in the *y* direction is given by

$$(EIv'')''+\rho A\ddot{v}=0 \tag{C.1}$$

where *E, I,* ρ, and *A* are the Young's modulus, area moment of inertia, density and cross sectional area, respectively. The displacement *V(t)* applied to the base of the beam in the *y* direction is given by

$$V(t)=v_0\cos(\Omega t) \tag{C.2}$$

wher v_0 is the maximum amplitude of the displacement at the base, and Ω the excitation frequency. The transverse displacement *v* of any point along the beam is given by

$$v=v_b+V(t) \tag{C.3}$$

where v_b is the displacement of the beam relative to the base. Substituting (C.3) into (C.1) yields

$$EIv_b^{iv} + \rho A(\ddot{v}_b - v_0\Omega^2 \cos(\Omega t)) = 0 \tag{C.4}$$

which can be written as

$$EIv^{iv} + \rho A\ddot{v} = f(x,t) \tag{C.5}$$

Equation (C.5) is a partial differential equation in the displacement relative to the base of the beam v_b. However, the subscript b is dropped for the sake of simplicity. The forcing function $f(x,t)$ in (C.5) is given by

$$f(x,t) = \rho A a_b \cos\Omega t \tag{C.6}$$

where a_b is the maximum amplitude of the acceleration applied to the base of the beam, and is given by

$$a_b = v_0\Omega^2 \tag{C.7}$$

The dynamic system for the problem described by equation (C.5) is shown in Figure C.2.

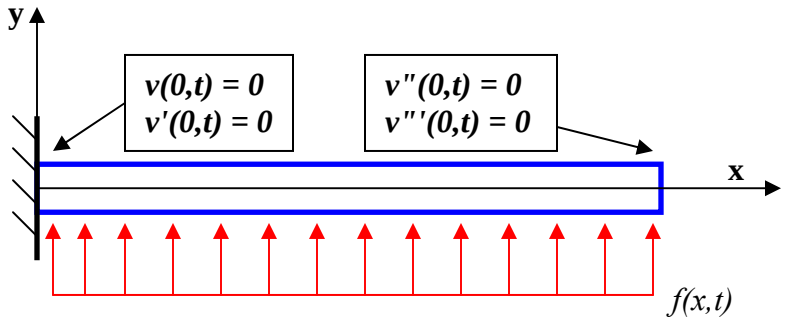

Figure C. 2: Cantilever beam with boundary conditions

The transverse displacement relative to the base of the beam is assumed as

$$v(x,t) = \sum_r {}^*V_r(x) q_r(t) \tag{C.8}$$

where ${}^*V_r(x)$ are the normalized mode shapes derived in Appendix B. Substituting (C.8) into (C.5) , multiplying the resulting expression by ${}^*V_s(x)$, and integrating over the length of the beam results in

$$[EI\int_0^l {}^*V_s\,{}^*V_r^{iv}\,dx]q_r + [\rho A\int_0^l {}^*V_s\,{}^*V_r\,dx]\ddot{q}_r = \int_0^l {}^*V_s f(x,t)dx \tag{C.9}$$

The mode shapes are orthonormal and obey the following relations (Thomson, 1998)

$$EI\int_0^l {}^*V_s\,{}^*V_r^{iv}\,dx = \omega_r^2\delta_{rs} \quad , \qquad \rho A\int_0^l {}^*V_s\,{}^*V_r\,dx = \delta_{rs} \tag{C.10}$$

where δ_{rs} is the Kronecker delta. Substituting (C.10) into (C.9) yields

$$\omega_r^2 q_r + \ddot{q}_r = Q_r(t) \tag{C.11}$$

with $Q_r(t)$ given by

$$Q_r(t) = \int_0^l {}^*V_r f(x,t)dx \tag{C.12}$$

The solution of (C.11) is given by (Zill, 1997)

$$q_r(t) = a_r \sin(\omega_r t) + b_r \cos(\omega_r t) + \int_0^t Q_r(\tau)h(t-\tau)d\tau \tag{C.13}$$

where the third term is (C.13) is the convolution integral (Thomson, 1998). The quantity $h(t-\tau)$ in the third term of (C.13) is the unit impulse response of (C.11) and is given by

$$h(t-\tau) = \frac{1}{\omega_r}\sin[\omega_r(t-\tau)] \tag{C.14}$$

Substituting (C.14) and (C.12) into the convolution integral yields

$$\int_0^t Q_r(\tau)h(t-\tau)d\tau = \frac{\rho A a_b}{\omega_r}\int_0^l {}^*V_r dx \int_0^t \cos(\Omega t)\sin[\omega_r(t-\tau)d\tau = F_1^r F_2^r \tag{C.15}$$

with F_1^r and F_2^r defined as

$$F_1^r = \int_0^l {}^*V_r dx \ , \qquad F_2^r = \frac{\rho A a_b}{\omega_r}\int_0^t \cos(\Omega t)\sin[\omega_r(t-\tau)d\tau \tag{C.16}$$

The initial conditions for this problem are given by

$$v(x,0) = 0 \ , \ \ \dot{v}(x,0) = 0 \tag{C.17}$$

Substituting (C.17) into (C.13) yields

$$a_r = 0 \, , \ \ b_r = -F_1^r \frac{\rho A a_b}{\omega_r}\left[\frac{1}{2(\omega_r - \Omega)} + \frac{1}{2(\omega_r + \Omega)}\right]$$

(C.18)

Therefore q_r is given by

$$q_r(t) = b_r \cos(\omega_r t) + F_1^r F_2^r \tag{C.19}$$

and the beam response is obtained by substituting (C.19) into (C.13).

Appendix D: Calculation of ki_{ij}

The procedure used to calculate the inertial nonlinear stiffness matrix ki_{ij} is illustrated through a simple example. A similar procedure is used to calculate the curvature nonlinear stiffness matrix kc_{ij}, and the gravitational effect vector g_i.

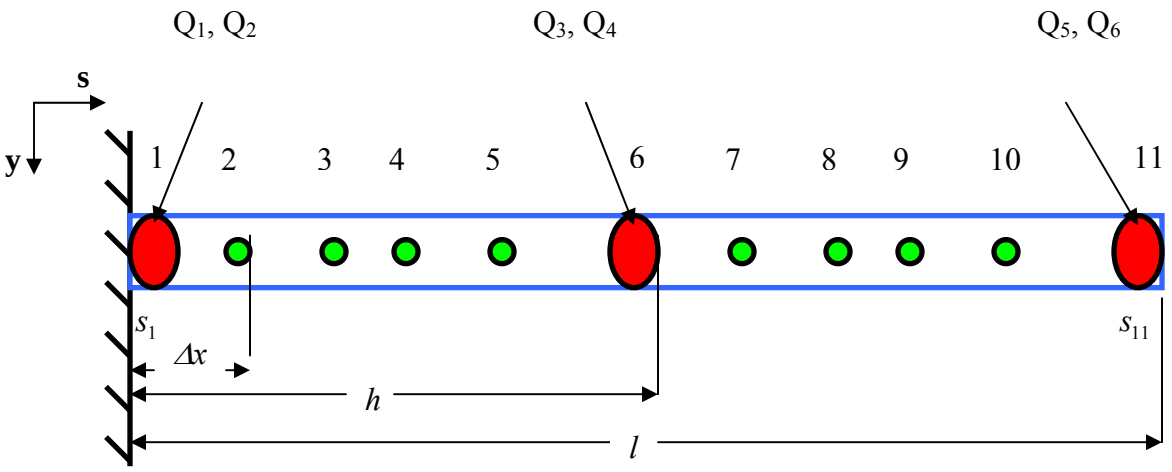

Figure D. 1: Two-element mesh for cantilever beam

For this example a cantilever beam of length l is meshed with two elements (Figure D.1) of length h each. Moreover, each element is divided into five smaller divisions of length Δx, resulting in a total of six grid points per element. The nodal displacements Q_j $(j=1...6)$ were obtained using the Newmark technique discussed in section 3.3.1.

Recall from Chapter 3, the inertial nonlinear stiffness matrix ki_{ij} (3.14) is defined in terms of the function f_2, which is given by

$$f_2 = \frac{\partial^2}{\partial t^2} \int_l^s \int_0^s v'^2 \, ds ds \tag{D.1}$$

where v is the transverse displacement in the y direction (Figure D.1). The order of differentiation and integration in (D.1) can be reversed, since these operators conmute (Kreyszig, 1999). Hence, f_2 is written as

$$f_2 = \int_l^s \int_0^s \frac{\partial^2 v'^2}{\partial t^2} ds ds \tag{D.2}$$

Equation (D.2) is evaluated numerically in three steps. The second derivative of v'^2 with respect to time is calculated first, followed by the first integral from *0* to *s*, and finally the second integral from *l* to *s*. These steps are discussed in detail next.

In order to evaluate f_2 using (D.2) the spatial derivative of the transverse displacement v needs to be estimated. The transverse displacement is approximated as

$$v \approx \sum_{e=1}^{2} \widetilde{V}^e(s,t) \tag{D.3}$$

where $\widetilde{V}^e(s,t)$ is the displacement inside the element given by

$$\widetilde{V}^e(s,t) = \sum_{j=1}^{4} \psi_j(s) Q_j^e(t) \qquad e = 1,2 \tag{D.4}$$

with the shape functions given by (Reddy, 1993)

$$\psi_1 = 1 - 3\left(\frac{s}{h}\right)^2 + 2\left(\frac{s}{h}\right)^3, \quad \psi_2 = h\left[\left(\frac{s}{h}\right) - 2\left(\frac{s}{h}\right)^2 + \left(\frac{s}{h}\right)^3\right],$$
$$\psi_3 = 3\left(\frac{s}{h}\right)^2 - 2\left(\frac{s}{h}\right)^3, \qquad \psi_4 = h\left[-\left(\frac{s}{h}\right)^2 + \left(\frac{s}{h}\right)^3\right] \tag{D.5}$$

Substituting (D.4) into (D.3) yields

$$v \approx \sum_{e=1}^{2} \sum_{j=1}^{4} \psi_j(s) Q_j^e(t) \tag{D.6}$$

which is used to calculate the spatial derivative of the transverse displacement.

$$v' \approx \sum_{e=1}^{2} \sum_{j=1}^{4} \frac{\partial \psi_j(s)}{\partial s} Q_j^e(t) \tag{D.7}$$

The second time derivative of v'^2 in the interval [0,TF] ,where *TF* is an arbitrary time, is calculated next. Figure D.2 shows the time nodes in the interval [0,TF], where *j* is the time node index.

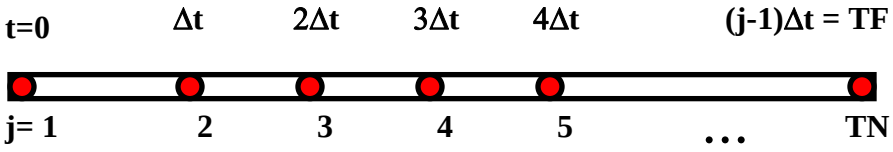

Figure D. 2: Time nodes in [0,TF]

The number of time nodes in [0,TF] is given by

$$TN = \frac{TF}{\Delta t} + 1 \tag{D.8}$$

The second derivative of v'^2 with respect to time for an arbitrary node in [0,TF], such that $1 < j < TN$, is calculated using the central difference formula (Kreyszig, 1999). Thus, the second time derivative of v'^2 is given by

$$J_j(s) = \left. \frac{\partial^2 v'^2}{\partial t^2} \right|_j = \frac{^{j+1}v' - 2^j v' + ^{j-1}v'}{\Delta t^2} \tag{D.9}$$

where ${}^{j+1}v'$, ${}^{j}v'$ and ${}^{j-1}v'$ are the values of the function v' evaluated at time nodes *j+1, j,* and *j-1*, respectively.

The second derivative with respect to time of v'^2 for node 1 in [0,TF] is approximated using the linear transverse transient displacement solution of a cantilever beam given by

$$v(s,t) = \sum_r {}^*V_r(s)[b_r \cos(\omega_r t) + F_1^r F_2^r(t)] \tag{D.10}$$

The ${}^*V_r$ are the normalized modes for the linear problem given by (B.12). The quantities b_r, F_1^r , and $F_2^r(t)$ are defined in Appendix C. The second derivative of v'^2 with respect to time for node 1 *(j=1)* in [0,TF] is then

$$J_j(s) = \left.\frac{\partial^2 v'^2}{\partial t^2}\right|_j = 2(v'\ddot{v}'+(\dot{v}')^2) \qquad j=1 \tag{D.11}$$

where (D.10) is used to calculate the required derivatives of v.

Now that the expressions for the second time derivative of v'^2 for all the nodes in [0,TF] are defined, f_2 is given by

$$f_2 = \int_l^s \int_0^s J(s)dsds \tag{D.12}$$

Notice the subscript j has been omitted in (D.12) for the sake of simplicity. Equation (D.12) is evaluated numerically for all eleven grid points along the beam (Figure D.1). The numerical integration of (D.12) is illustrated next.

For any grid point along the beam, f_2 is given by

$$f_2(s_k) = \int_l^{s_k} \int_0^{s_k} J(s) ds ds \qquad k = 1...a \tag{D.13}$$

where s_k is the k^{th} grid point in Figure D.1; and a is the total number of grid points along the beam, eleven for this example. Both integrals in (D.13) are evaluated using Simpson's rule. The first integral in (D.13) is calculated as (Borse, 1997)

$$I_1(s_k) = \int_0^{s_k} J(s) ds = \frac{s_k}{3(k-1)} [J(0) + 4 \sum_{\substack{i=2 \\ even \quad i}}^{k-1} J(s_i) + 2 \sum_{\substack{i=3 \\ odd \quad i}}^{k-2} J(s_i) + J(s_k)] \tag{D.14}$$

Finally, f_2 is calculated as (Borse, 1997)

$$f_2(s_k) = \int_l^{s_k} I_1(s) ds = \frac{s_k - l}{3(a-k)} [I_1(l) + 4 \sum_{\substack{i=1 \\ even \quad i}}^{a-k-1} I_1(s_{k+i}) + 2 \sum_{\substack{i=2 \\ odd \quad i}}^{a-k-2} I_1(s_{k+i}) + I_1(s_k)] \tag{D.15}$$

The function f_2 given by (D.13) is finally used to calculate the element inertial nonlinear stiffness matrices

$$ki_{ij}^1 = \frac{1}{2} \rho A \int_0^h \psi'_i \psi'_j f_2(s) ds \qquad 0 < s < s_6 \tag{D.16}$$

$$ki_{ij}^2 = \frac{1}{2} \rho A \int_0^h \psi'_i \psi'_j f_2(s) ds \qquad s_6 < s < l \tag{D.17}$$

where ρ , A, and l are the density, cross sectional area, and length of the beam, respectively. The range for s in (D.16) and (D.17) is defined from Figure D.1. Assembly of the two element matrices (D.16) and (D.17) yields the global inertial nonlinear stiffness matrix ki_{ij}. The integration in (D.16) and (D.17) is done using Simpson's rule.